FINAL TECHNICAL REPORT

Project Title: New Cyclotron Targetry to Enhance F-18 Clinical Position Emission Tomography

Covering Period: Aug 15, 2004 - Aug 14, 2008

Date of Report: December 19, 2008

Recipient: North Carolina State University, Raleigh NC 27695-7909

Award Number: DE-FG07-04ID14593

Subcontractors: --------

Other Partners: --------

Contact(s): J. Michael Doster, 919-515-3658, doster@eos.ncsu.edu

Project Team: Nancy Elizondo, US DOE, Idaho Operations Office

Project Objective: This project proposes to develop cyclotron targets that produce F-18 for clinical Positron Emission Tomography (PET) at significantly higher rates than that available from current targetry. The production rate of ^{18}F is directly proportional to the beam current. Higher beam currents would result in increased ^{18}F production but would be accompanied by higher heat loads to the target. The beam power available in most commercial cyclotrons exceeds the heat removal capacity of current target technology by a factor of two to four, significantly limiting the production rate of Fluorine-18.

The purpose of this project is to design and test targets that can withstand higher beam currents/higher incident proton energies thus producing higher yields of ^{18}F for use in medical imaging scans.

Background: The research project was funded under the NEER program to support nuclear engineering education and research. One graduate student was supported ½-time. Dr. Matt Stokely completed a Masters Degree in December of 2006 and his PhD degree in Nuclear Engineering in May of 2008.

Two target types were considered, thermosyphon batch targets and a recirculating target where the heated target water is pumped to a heat exchanger, cooled and returned to the target.

Themosyphons are simple gravity driven devices that can achieve high heat transfer rates through the transfer of latent heat. A typical design involves a boiler or evaporator section where the working fluid

boils. The vapor flows upward to a condenser section where the vapor condenses on the walls of the thermosyphon and flows back to the evaporator section. Thermosyphon target designs were tested at the Duke Medical Center and the Wisconsin Medical Center cyclotron and indicated performance levels in excess of 2 kW. Predictive models of thermosyphon target performance have also been developed and benchmarked against experimental results. These predictive models have been used to produce the next generation thermosyphon target designs.

The recirculating target design assumes no net boiling within the target. The heated water is pumped from the target body to an external heat exchanger, where the target water is cooled and returned to the target chamber. Due to its high cost, a major design constraint for the recirculating target is minimizing the volume of ^{18}O water contained within the system. A prototype recirculating target consisting of target body, compact heat exchanger and miniature turbine pump has been designed, fabricated and tested. Analysis of this first design suggested heat rejection capabilities in excess of 4 kW while operating at atmospheric pressure. Performance models of the recirculating target have been produced and used to increase the performance of these targets. Significant effort has gone into the design of low volume, high capacity compact heat exchangers for the recirculating target. Current designs suggest heat rejection capabilities in excess of 10 kW at relatively low operation pressures (100 psia).

Deployment, Testing and Analysis of Advanced Thermosyphon Target Systems for Production of Aqueous [^{18}F]Fluoride via ^{18}O(p,n)^{18}F

Abstract

Production of Aqueous [^{18}F]Fluoride for Positron Emssion Tomography (PET) can be improved with advanced target designs. Single phase and boiling batch water targets are the most common designs for the cyclotron production of ^{18}F via the ^{18}O(p,n)^{18}F reaction. Thermosyphon targets have design and operating characteristics which enable higher power operation than conventional boiling targets of like size. Experimental thermosyphon target systems demonstrated the feasibility of high intensity irradiation via bottom pressurized operation. An effective experimental characterization platform was developed and utilized in parallel with computational modeling efforts to further improve designs[1,2]. A control strategy was also developed to provide a simple and robust means of remote target operation. Clinical production systems were designed and deployed at two facilities.

Fundamentals of Liquid Targets

The function of a production accelerator target is the transmutation of a stable element into a product radionuclide via bombardment with high energy particles. The specific target geometry and implementation are the product of many disciplines including chemistry, nuclear physics, and thermodynamics. In the case of $^{18}F^-$ production, the target medium is [O-18] enriched water. A liquid target is constructed of, principally, three components:

1. A chamber containing the target medium;
2. A foil window that is strong enough to confine the medium within the chamber, yet thin enough to allow particles to pass through with an acceptable loss of energy;
3. A target body that houses the chamber and window, which connects to a beam line or port and provides a path for coolant to remove waste heat from the system.

A simplified target drawing is included to highlight these features (Figure 1). The target chamber shown has a racetrack shape. This has been the geometry of choice for boiling water targets since the inception of the PET cyclotron. It is intended to accommodate boiling in the lower region of the chamber, where the beam enters the target. The area above the beam strike provides a vapor space, or condenser. This geometry has been utilized in both traditional reflux and thermosyphon targets. The production capacity of any target system is a function of beam energy and current. Waste heat is generated by the protons as they slow down in the target. If the heat input is greater than the thermal capacity of the system, vapor voids in the beam strike can lead to particles fully penetrating the target medium. If the protons do not stop in the target medium, but rather in the target body, radionuclide production will suffer. Consequently,

the design and development of target systems with increased heat removal capabilities is one way to expand production capacity.

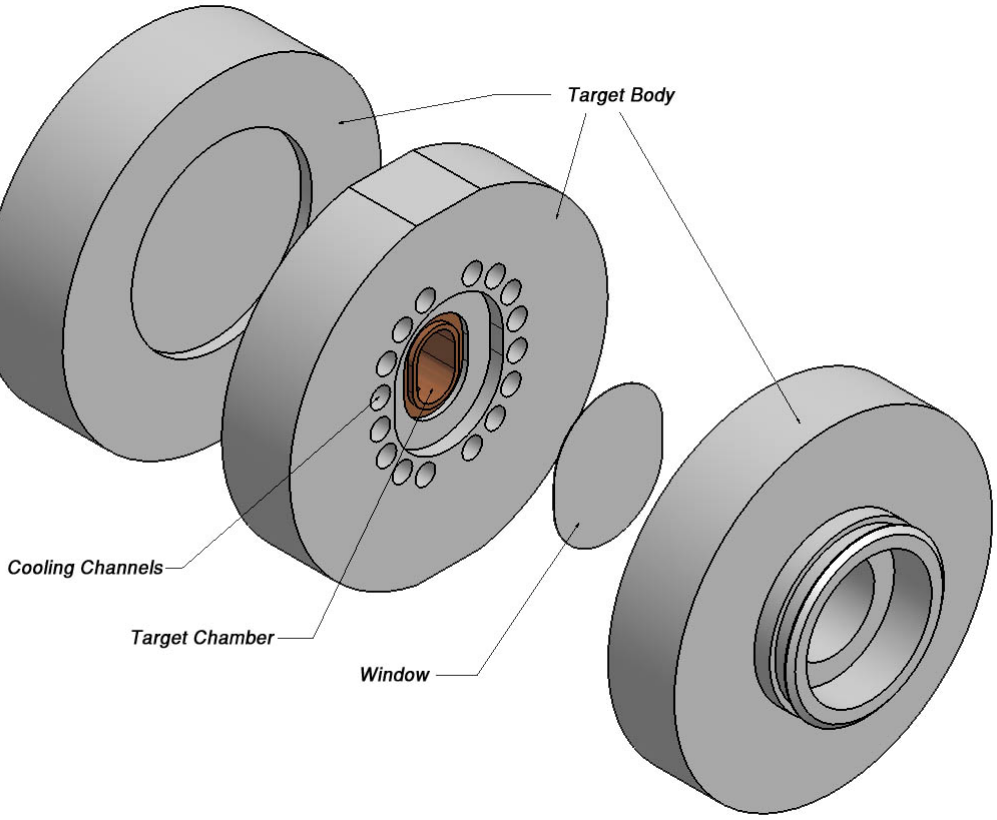

Figure 1: Principal Liquid Target Components

The most important metric for target performance is the production capability of F-18 and, ultimately, ^{18}FDG. This can be evaluated by comparison with a theoretical thick target saturation yield (TTY) value which is equivalent to the reaction rate. This rate can be computed directly from the cross section of the nuclear reaction of interest and the stopping power of the incident particle as a function of energy using the following method.

Consider a perfectly collimated beam of protons with initial energy E_0 and intensity ϕ_0 incident upon an infinite homogeneous cylindrical volume of target material. The distribution of particles inside the target volume can be represented as

$$\phi(x, E') = \phi_0 \delta(E' - E(x)) \tag{1}$$

for all energies E' and beam energies E(x), given implicitly by the stopping power

$$E(x) = E_0 - \int_0^x \frac{dE}{dx'}\big(E(x')\big)dx' \tag{2}$$

This assumes that the energy-integrated intensity of particles does not have any spatial dependence, and is valid if the energy threshold of the reaction of interest is significantly higher than the Bragg energy.

The reaction rate inside the volume can be expressed as

$$R = A\int_0^\infty\int_0^\infty \phi\left(x, E'\right)\Sigma\left(E'\right)dE'dx \tag{3}$$

where A is the cross sectional area of the cylinder. Substituting expression 1 yields

$$R = A\phi_0\int_0^\infty\int_0^\infty \delta\left(E' - E\left(x\right)\right)\Sigma\left(E'\right)dE'dx \tag{4}$$

$$R = A\phi_0\int_0^\infty \Sigma\left(E\left(x\right)\right)dx \tag{5}$$

This can be expressed in more convenient parameters of beam current and effective length

$$R = I_{beam}\int_0^L \Sigma\left(E\left(x\right)\right)dx \tag{6}$$

The integral is evaluated numerically by the approximation

$$R = I_{beam}\sum_{n=1}^{N}\Sigma\left(E\left(x_{n-1}\right)\right)\left(x_n - x_{n-1}\right) \tag{7}$$

Figure 2 was generated using the this approach as an example. The TTY for the $^{16}N(p,\alpha)^{13}N$ reaction is also included due to its usefulness in liquid target diagnostics, which will be discussed in a later section.

The SRIM 2003 software package can be used to generate stopping power tables for charged particles in a wide variety of target mediums. Using these values to generate the spatial energy distribution and the published excitation function for the cross sections, TTY values may be computed for most nuclear reactions of interest in medical isotope production.

As an alternate approach, the MCNPX code was also used to evaluate the effective reduction in yield. MCNPX is a general purpose Monte Carlo radiation transport code that is capable of simulating both neutral and charged particle transport in arbitrary geometries. When supplied with the excitation function, the code calculates the

volumetric reaction rate directly. No significant differences in computed yield resulted form the two different approaches.

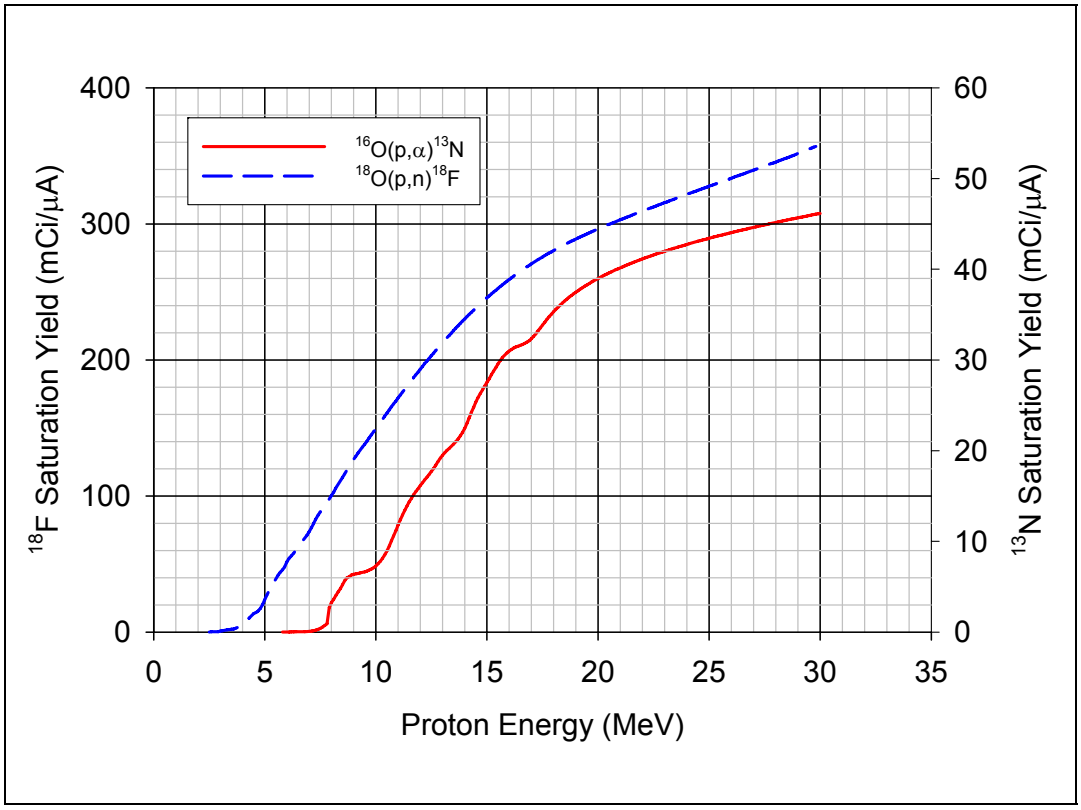

Figure 2: Theoretical Water Target Saturation Yields for ^{18}F and ^{13}N

Current Technology in Contrast to Thermosyphon Systems

Most liquid targets used for medical isotope production are pressurized from the top of the liquid volume. Three cyclotron manufacturers currently produce the overwhelming majority of the accelerators for the producing PET isotopes: CTI/SIEMENS (RDS-112, RDS-111), GE (PETtrace, MINItrace), and IBA (18/9). The production packages offered by these vendors utilize "reflux" targets of this type[3,4]. One limitation of top pressurization is that there exists an initial amount of non-condensable gas which mixes with the liquid and vapor during irradiation. Even a small component of non-condensable gas produces a dramatic increase in resistance to heat transfer at a condensing surface[5]. This is significant, as the condensing layer can become the limiting resistance when the target is cooled more aggressively.

In contrast, a thermosyphon target is initially filled completely and pressurized from the bottom via an external expansion volume. This technique is intended to better utilize the effective heat transfer area in the condensing region of the target volume by

eliminating the presence of non-condensable gas. Many experimental targets of this type have been developed in previous work, of which the most aggressive designs achieved operation at power levels in excess of 3 kW[6]. Both types of targets are self-regulating, in that the vapor generated will occupy the amount of condensing surface area necessary to reject the incident beam power.

Experimental Methods

Comparing the TTY for an irradiation to theoretical values gives an excellent indication of beam fluence in the target medium. Irradiations can be performed using either natural abundance water or [^{18}O]enriched water. Natural abundance water offers the advantage of low cost, and the production of ^{13}N via ^{16}O(p,α)N^{13} can be used for diagnostic purposes. For proton energies above 16 MeV ^{15}O is produced via ^{16}O(p,pn)^{15}O and must be included in calculations. Enriched water is more costly, but produces little activity from isotopes other than ^{18}F (with the exception of ^{17}F which has a half life of approximately one minute and will have decayed by the time product is delivered in most cases) and simplifies analysis. Another advantage of enriched water is that the [^{18}F] fluoride activity can be synthesized into FDG, which gives an indication of the chemical quality of the product.

Finding the optimum intensity at which to run a target is accomplished by many irradiations on both natural abundance and enriched material. This is an expensive and time consuming process. While it yields critical information, it does not provide a complete picture of the physical processes in the target. For this reason, it is important to measure other physical parameters.

Vapor fraction in the beam strike is the most critical parameter concerning target penetration. Though the local vapor fraction in the proton beam cannot be measured directly, the target averaged vapor fraction can be measured by means of a glass sight tube. This diagnostic method is not unique to the Thermosyphon target but easily cannot be implemented in the case of top pressurized operation. The sight tube is attached between the expansion chamber and helium supply valve and has an internal diameter and length appropriate for the target fill volume. The target is filled until water is visible in the sight tube, pressurized, and irradiated. An illustration of the sight tube before and during irradiation is included in Figure 3.

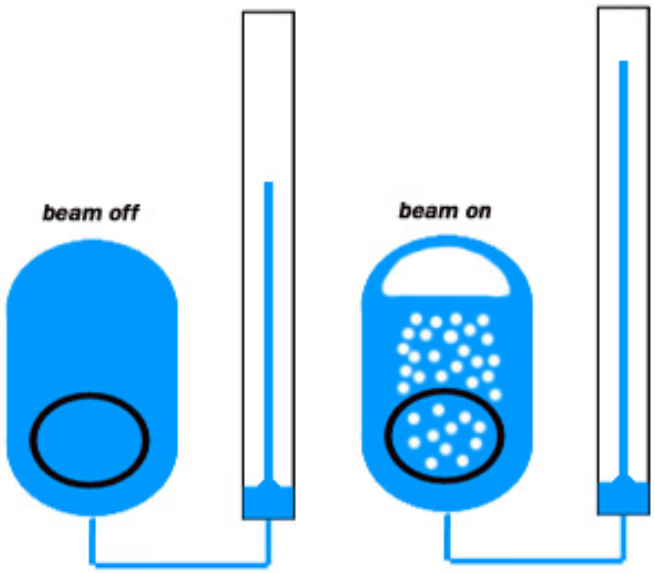

Figure 3: Sight Tube Connected to Bottom of Target

The regions of operation can be observed by inspecting the sight tube level as a function of beam current. The operating modes are listed below:

1. Single Phase Convection – linear rise in level from thermal expansion
2. Subcooled Window Boiling – minute erratic level movement
3. Subcooled In-Beam Boiling – small level oscillations
4. Bulk In-Beam Boiling – regular level oscillations with magnitude proportional to beam intensity
5. Penetration (controlled) – maximum level plateaus while minimum level continues to rise
6. Penetration (severe) – violent swings in level (frequency and displacement)

Each of these modes corresponds to a specific time dependent behavior of the internal target pressure. This can be observed by installing a pressure transducer between the chamber and expansion volume. Analysis of the boiling kinetics has been reserved for future work. It should be noted that true thermosyphon boiling has yet to be observed in any target, presumably due to the small chamber dimensions. Controlled penetration has been seen in targets tested at Wisconsin Medical Center (WMC), while the Duke University Medical Center (DUMC) targets transitioned directly from bulk boiling to severe penetration. These experiments will be discussed further in the research summary.

Penetration results from insufficient target mass along the proton track. Charged particle transport is well understood and proton ranges can be calculated for a variety of

compounds, energies and geometries. Range thickness values have been calculated for volume averaged two phase distributions (Figure 4).

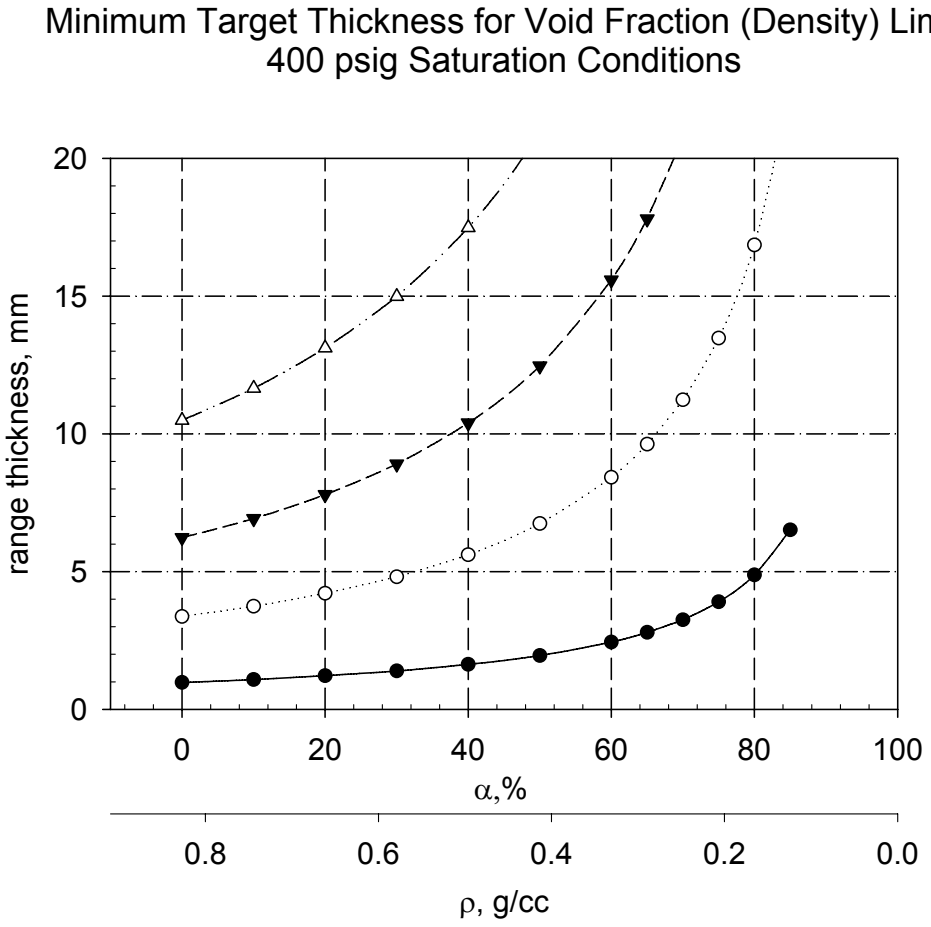

Figure 4: Range Thickness as a Function of Average Void Fraction

The uncertainty in range thickness for a boiling target results from the distribution of liquid and vapor in the beam path. For any target operating at steady state, there exists a slight imbalance between the vapor generation and condensation rates. This is the product of small system volume and a volumetric heat input that is spatially dense. The imbalance is evident by the oscillations in the sight tube level. Phenomenological models can accurately predict heat transfer using a time-averaged value of target void fraction. However, the effective proton range is significantly less than would be expected for this average value due to variations in beam strike void. Determining the appropriate design margin for target depth is a high priority task for computational efforts in this area.

Pressure versus flow measurements were taken for the experimental targets. These data were used primarily for calculating heat transfer coefficients in computational

models. Additionally, inlet and exit temperatures were measured and total heat transfer from the target by cooling water was directly measured.

Experimental Results and Clinical Deployment

Recent work has focused on scaling thermosyphon technology to suit specific cyclotron applications. Robust production systems have been developed for a TCC CS-30 at the Duke University PET Facility (DUMC) and a GE PETtrace known as the Wisconsin Medical Cyclotron(WMC). In these systems, the chamber and window materials are tantalum and Havar, respectively. The goal of these deployments was to provide target systems very closely matched in thermal capacity to the current limit of the cyclotrons.

The DUMC cyclotron has an extracted proton energy of 26 MeV and current capability of 45 μA (1170W). In the past, reflux production targets were operated at lower proton energies, which required attenuation of the particle beam. In order to achieve the maximum possible ^{18}F production, the thermosyphon target was designed to operate at full energy. The TS6-DUKE target has a depth of 15 mm, a target chamber diameter of 10 mm and an internal volume of approximately 1.93 mL. The addition of the thermosyphon system has more than doubled the ^{18}F capacity of the facility. This target has been operated exclusively without a component failure or disassembly for cleaning since its installation in 2007.

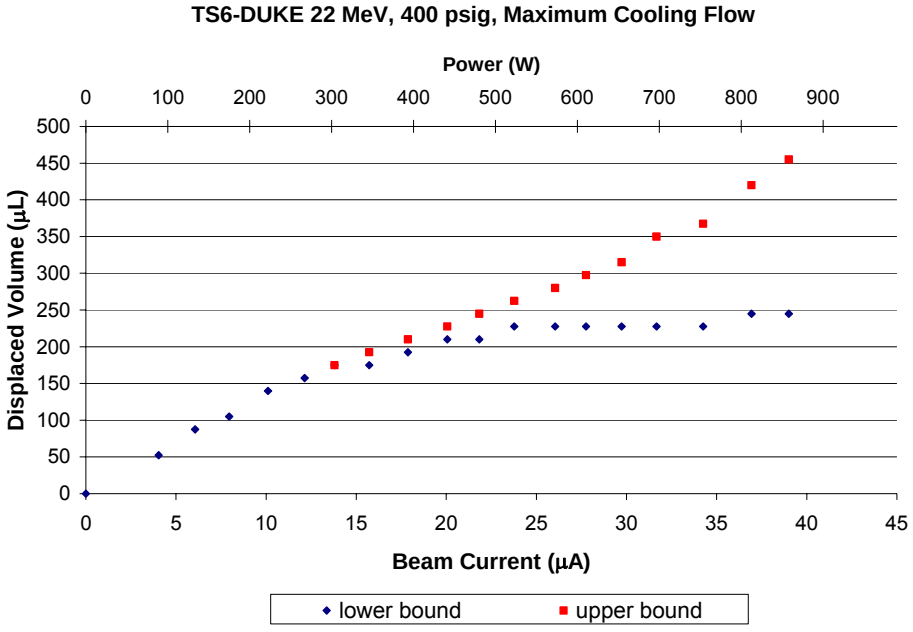

Figure 5: Sight Tube Data for Normal Operating Parameters

Sight tube data were collected under full cooling flow conditions and an overpressure of 400 psig. These would be the typical parameters for daily production. Under these conditions, the target does not exhibit behavior indicative of penetration at

beam currents up to 40 μA (880 W), the maximum output available for the CS-30 at the time. Sight tube measurements are included in Figure 5.

These data suggest that the target is operating in a bulk boiling mode above approximately 22 μA. The maximum displaced volume increases with intensity but in a steady, controlled fashion. Without the capacity to run at higher beam current, the ultimate performance limit cannot be determined. However, operation up to 1 kW appears reasonable. The TS6 system has been successfully qualified for clinical production at the Duke PET facility. A set of production curves are included inFigure 6.

These calculations assume a conservative saturation yield of 280 mCi/μA. The implementation of this target system will both increase the total production capacity of the site and add operational flexibility. This is very important with the addition of new scanners and an increased patient load. Producing clinical doses in less time also creates production space for experimental processes and compounds used for research.

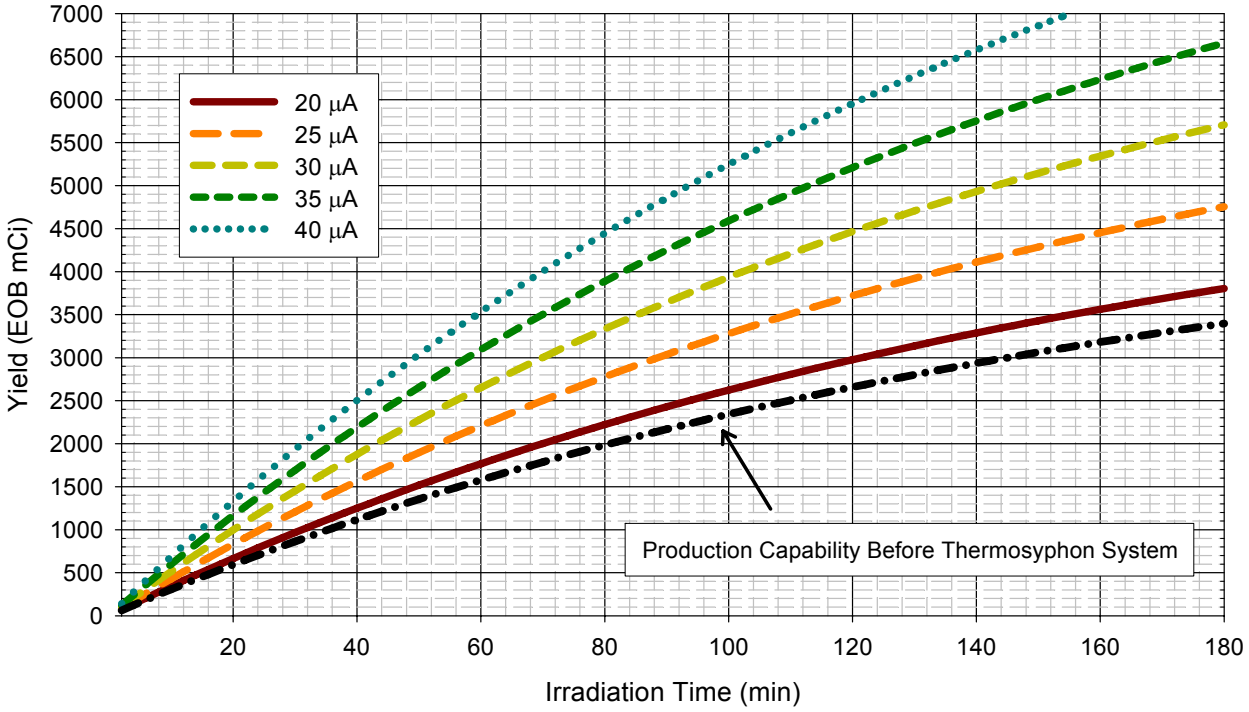

Figure 6: DUMC Thermosyphon Production Curves

Production data from the first two months of service are included Figure 7. Some fluctuation in ^{18}F saturation yield values is the result of a minor contribution of ^{17}F activity in the first production of each day, which can be extremely short (<20 minutes). The 18FDG yield values are much more consistent, as would be expected. A solid model and photograph of this target is included in

Figure 8.

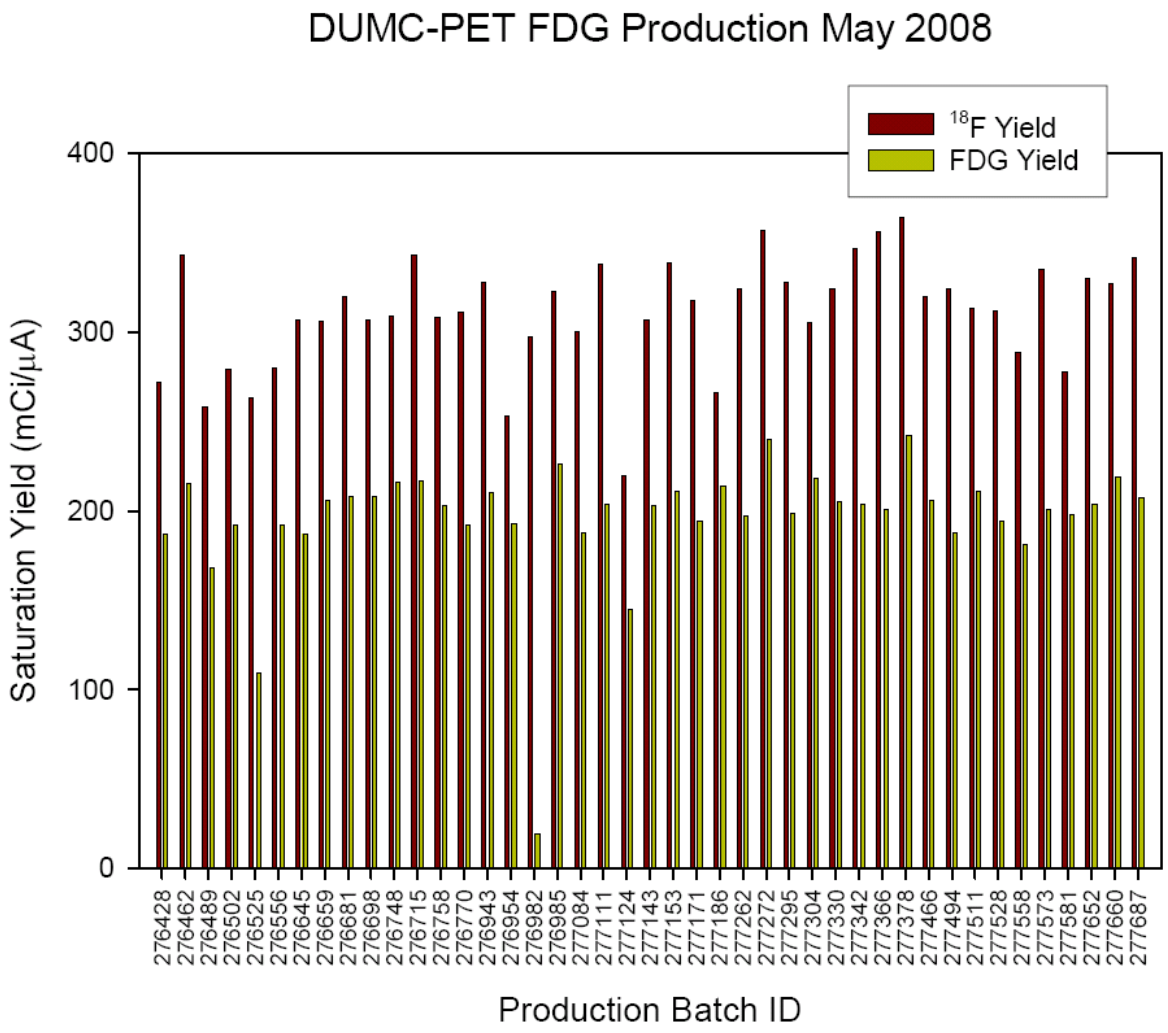

Figure 7:Clinical Production Data for TS6-Duke Thermosyphon

The WMC facility typically operates two GE high yield reflux targets simultaneously via dual beam extraction. The thermosyphon target for this application was designed to tolerate beam currents approaching 100 µA (1650W), corresponding to the software limit for automated cyclotron operation. The TS6-WMC target has a depth of 15 mm, a target chamber diameter of 15 mm and an internal volume of approximately 4.3 mL. The target was first installed in concert with a D-PACE short port collimator assembly to characterize the beam profile at the vacuum tank exit port[7].

Sight tube data were collected at a beam energy of 16.5 MeV and an overpressure of 400 psig. These experiments were performed from the PETtrace service computer which permits higher power operation but removes many protective interlocks. The limiting component for this mode of operation is the radiofrequency power supply, which cannot exceed 15 kW. This corresponds to roughly 150 µA of beam at the exit port. After transmission losses through the collimators, it was possible to obtain a maximum of 125 µA on target.

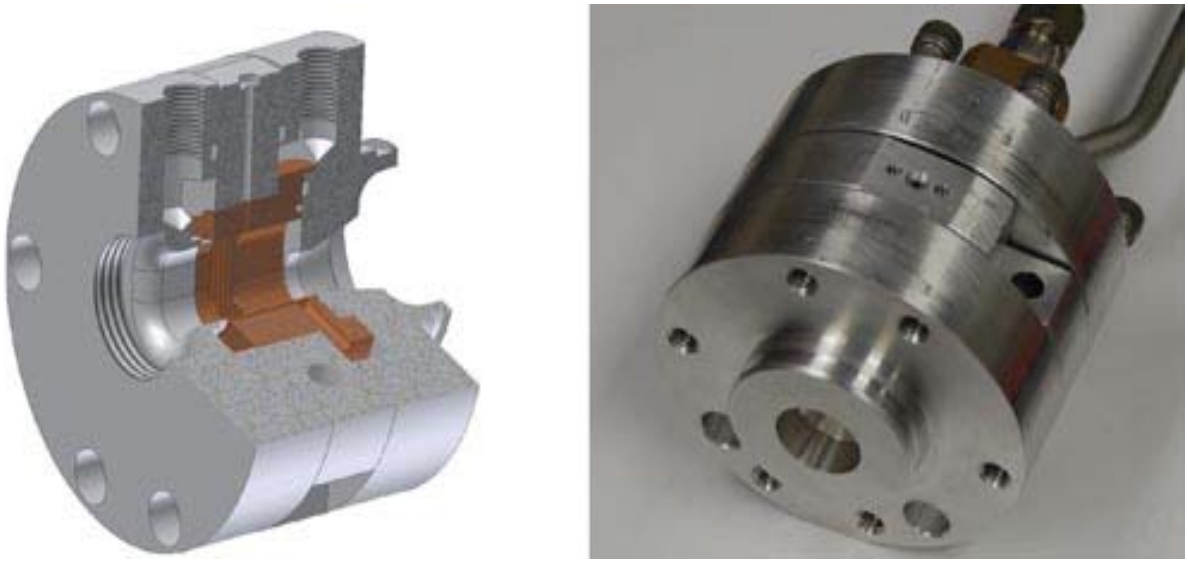

Figure 8: DUMC Thermosyphon Solid Model and Assembled Target

The target exhibits typical behavior in the thermal expansion, subcooled boiling and bulk boiling modes up to 110 μA (1760 W). Above this power level, the incremental rise in sight tube level becomes smaller with respect to constant increases in current(Figure 9). It was initially hypothesized that this behavior results from an increase in condenser void fraction and the subsequent increase in condensing heat transfer coefficient. Later targets have since shown this behavior very close to the onset of target penetration. While the target insert exhibited some discoloration, it was not clear that significant penetration had occurred. Yield tests at these elevated currents have confirmed that indeed target penetration had occurred.

The WMC thermosyphon system has been successfully qualified for clinical production. A set of production curves are included in 10. These calculations assume a conservative saturation yield of 230 mCi/μA. The implementation of this target system will increase the production capacity of the facility by more than 50 percent. In addition, the total production time is reduced, potentially resulting in longer maintenance intervals for some cyclotron components.

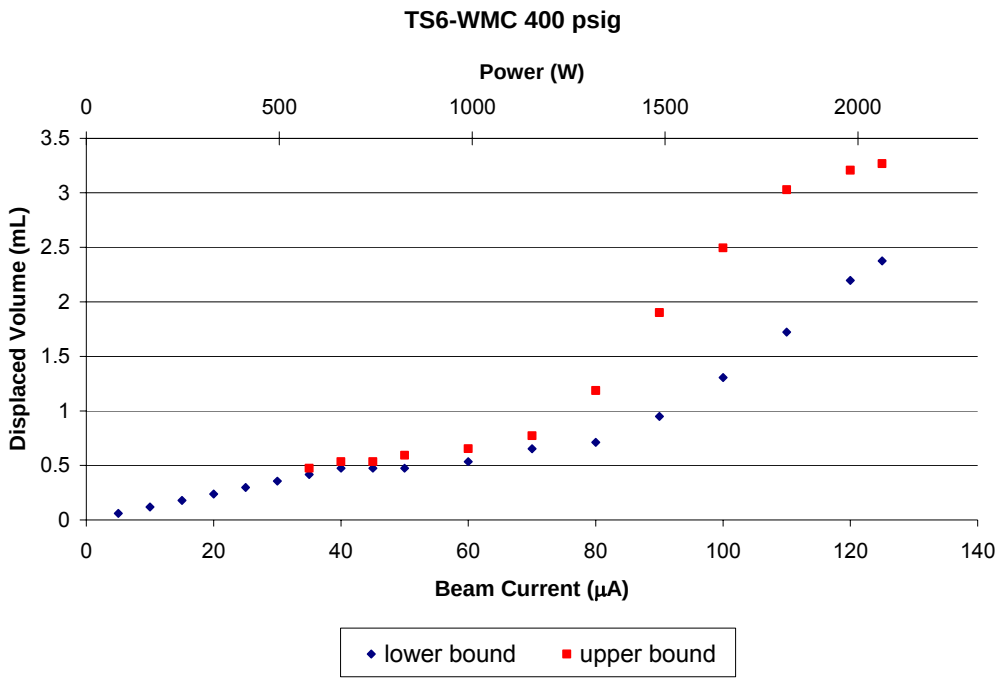

Figure 9: TS6-WMC Sight Tube Data

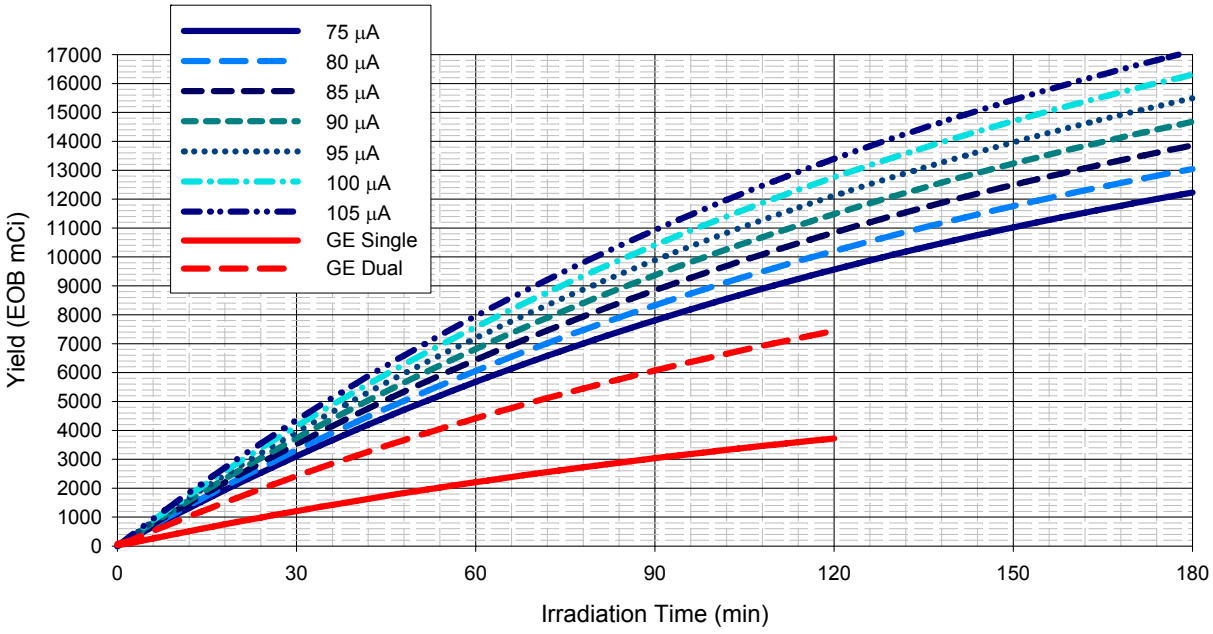

Figure 10: WMC Thermosyphon Production Curves

Saturation yields for ^{18}F as well as ^{18}FDG are both higher and more consistent than with the stock target package. In addition to operation at high intensity, the target has demonstrated consistent saturation yield performance for extended irradiation times (>4hr). Sample production data are included in Figure 11. High current production has not yet been needed, but test irradiations have been performed at 100 μA with no decrease in saturation yield.
Figure 12 includes a solid model and a photograph of the target.

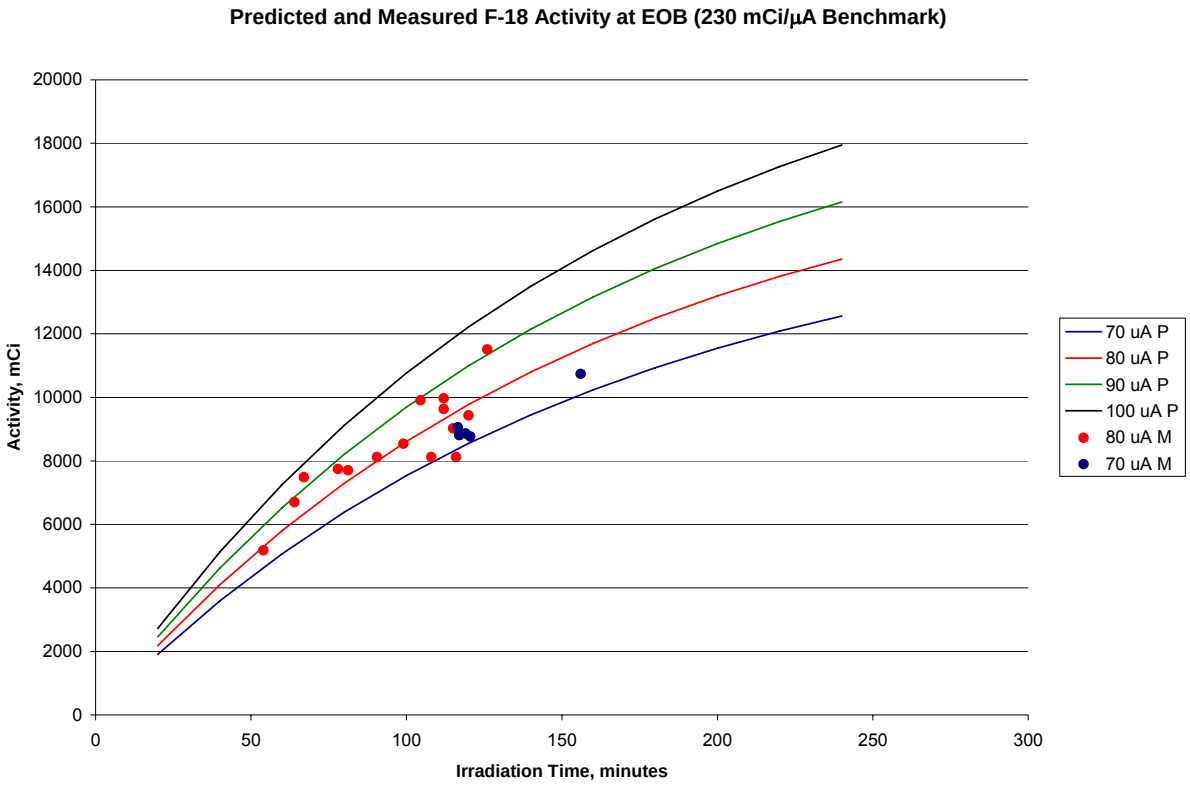

Figure 11: WMC Thermosyphon Production Data

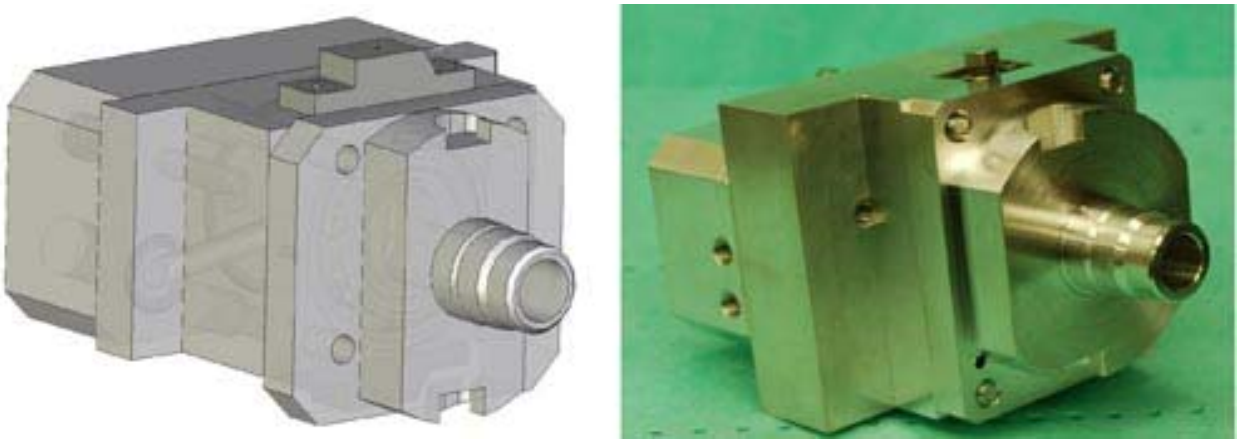

Figure 12: WMC Thermosyphon Solid Model and Assembled Target

REFERENCES

1. Stokely M.H., Deployment, Testing and Analysis of Advanced Thermosyphon Target Systems for Production of Aqueous [^{18}F]Fluoride via ^{18}O(p,n)^{18}F. Doctor of Philosophy Dissertation, Department of Nuclear Engineering North Carolina State University. Raleigh, North Carolina: 2008.
2. Peeples J.L., Design and Testing of Thermosyphon Batch Targets for Production of ^{18}F. Doctor of Philosophy Dissertation, Department of Nuclear Engineering, North Carolina State University. Raleigh, North Carolina: 2008.
3. Eriksson T. *et al*, "Using a niobium water target on the PETtrace cyclotron producing 18F-." *Proceedings of the Eleventh Workshop on Targetry and Target Chemistry*. Cambridge, UK: 2006.
4. Alvord C.W. *et al*, Design, test and widespread implementation of a compact kilo-Watt fluoride ion target. *Nuclear Instruments and Methods in Physics Research B*. 241:708-712, 2005.
5. Collier J.G., Convective Boiling and Condensation. UK: McGraw Hill, 1981.
6. Stokely M.H. *et al*, "High Yield Thermosyphon Targets for Production of 18F-Fluoride," *Proceedings of the Eleventh Workshop on Targetry and Target Chemistry*. Cambridge, UK: 2006.
7. Theroux J.E. *et al*, "A 'Short Port' Beamline for Mounting Custom Targets to a PETtrace™ Cyclotron." *18th International Conference on Cyclotrons and their Applications*. Giardini Naxos, Italy: 2007.

Thermal Modeling of Batch Boiling Water Targets for $^{18}F^-$ Production

Abstract

Batch boiling targets are commonly used in cyclotrons to produce Fluorine-18 by proton bombardment of Oxygen-18 enriched water. Computational models have been developed to predict the thermal performance of thermosyphon production targets. The models have been validated with experimental test data from the Duke University Medical Cyclotron and the Wisconsin Medical Cyclotron. Good agreement has been observed between experimental measurements and model predictions of average target vapor fraction as a function of beam current and energy.

Introduction

Batch boiling water targets are commonly used to produce ^{18}F through the $^{18}O(p,n)^{18}F$ reaction by proton bombardment of ^{18}O-enriched water. Historically, design of batch boiling targets has been primarily empirical, which required a significant amount of trial and error, long lead times and no guarantee of an optimal design. Recently, there has been an increased interest in modeling of the thermal processes which drive target performance [1-4]. This modeling effort has led to the development of a fundamental approach to target design, which has been implemented to design new targets with enhanced production capabilities.

The production capacity of any target system is a function of beam energy and current. As protons slow down in the target water, they produce a significant quantity of waste heat. This heat must be removed from the system in order to support target operation. If the heat input exceeds the thermal capacity of the system, vapor voids in the beam strike can lead to protons fully penetrating the target medium. Any protons that do not stop in the target medium will be absorbed in the target body, and radionuclide production will suffer. Consequently, the design and development of target systems with increased heat removal capabilities can expand production capacity.

For range-thick targets, ^{18}F production is directly proportional to beam current. Accordingly, target production can be increased by optimizing the heat rejection capabilities of the target, and target performance considerations can be essentially reduced to a heat transfer problem. Computational models have been developed which describe heat transfer in boiling targets. These models were developed to predict target thermal performance and have been validated with experimental test data from the Duke University Medical Cyclotron and the Wisconsin Medical Cyclotron. These models allow target designers to predict the effects of changing target geometry and materials in the absence of, or with limited, expensive and time-consuming experiments.

Reflux target systems, which are pressurized from the top of the liquid volume and begin operation with an initial amount of non-condensable gas in the top of the target, are the industry standard in ^{18}FDG PET production. Bounding performance curves have

been predicted for reflux targets [5]. Even a small component of non-condensable gas produces an increase in resistance to heat transfer at a condensing surface [6]. This is significant, as the condensing layer can become the limiting resistance as the target is cooled more aggressively. Thermosyphon targets, however, are pressurized from the bottom via an external expansion volume, and the target chamber is flush with liquid water at the beginning of irradiation. This maximizes the effective heat transfer area in the condensing region of the target volume by eliminating the presence of noncondensable gas.

Target Geometry

Recent thermosyphon production targets feature aluminum target bodies with tantalum inserts for the target chamber and cooling systems. Racetrack-shaped target chambers, s featured in traditional reflux targets, have been favored because they provide additional volume above the beam strike where vapor may accumulate [2,7]. Havar™ [8] foil is used for target windows in all targets with a nominal thickness of 0.001". In some instances for the PETtrace targets, which have unsupported window radii of 13.5 mm and 15 mm, a 0.002" thick foil is used to provide additional pressure margin.

Because reflux-style targets are pressurized from the top and begin operation with an initial amount of non-condensable gas, they are believed to form a distinct vapor region in the top of the target chamber during operation, which allows water to condense on the top of the target chamber and flow down the walls. A thermosyphon target, however, is pressurized from the bottom via an external expansion volume and begins operation flush with liquid water. As bubbles begin to form, liquid is expelled from the target into the expansion volume. A significant amount of turbulent boiling occurs during target irradiation, but conditions in the chamber never lead to vertical stratification. For very high vapor volume fractions, boiling conditions in a thermosyphon target could evolve into vertical stratification; in practice however, beam penetration occurs before stratification develops. Target operation could continue under penetrating conditions, but this problem is eliminated by design of range-thick targets.

When a model is employed which assumes vertical stratification in a bottom-pressurized target, the volume averaged vapor fraction required by the model for target cooling does not match observed experimental values. When turbulent boiling throughout the volume is assumed, good agreement is observed between model predictions and experimental results. Experimental and computation results imply operation in a bulk boiling mode, which has led to a redesign of thermosyphon targets. In the absence of vertical stratification, a cylindrical target chamber, with a circular cross-section, is more volume-efficient than a chamber with a conventional racetrack-shaped cross-section.

Thermosyphon targets feature cooling of the target chamber by two independent systems. Radial coolant channels are located around the target chamber and run parallel to the target chamber and the direction of the beam. Additional cooling is provided by a water jet which impinges on the back of the target. Heat generated in the target chamber

is conducted through the body of the target and removed by either the radial coolant channels or the back jet. Although many commercial targets restrict cooling to the back of the target, the use of radial cooling can dramatically increase heat removal capacity for the same water volume. For thermosyphon targets, it has been shown that more than 80% of the total heat is removed by the radial channels with the remainder removed by the back cooling [3].

Four targets were used in the validation study, which feature different chamber dimensions, materials and coolant geometries. While three of the targets feature classic racetrack-shaped chamber cross-sections, the remaining target, WMC-2, features a circular chamber cross-section. Geometry of the four targets is described in Fig. 2 and Table 1.

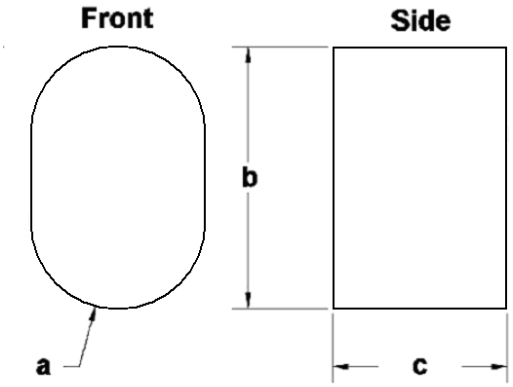

Figure 2. Target Chamber Dimensions

Table 1. Summary of Validation Targets

Target	Testing Facility	Material	Radius a (mm)	Height b (mm)	Depth c (mm)	Volume (mL)	Number of Channels	Diameter of Channels (in)
WMC-1	WMC	Silver	7.5	22.5	15.0	4.34	28	0.055
WMC-2	WMC	Aluminum	8.5	17.0	18.6	4.22	28	0.055
DUKE-1	Duke	Tantalum	5.0	15.0	15.0	1.93	10	0.136
DUKE-2	Duke	Tantalum	5.0	15.0	15.0	1.93	20	0.040

Target Materials

Silver has been a popular material for commercial water targets for the past 25 years, due to its high thermal conductivity (415 W/m K), ease of fabrication, and high oxidation resistance. Recently, tantalum has been proposed as a preferred target material because it is more inert and results in better quality fluoride ion, as well as longer intervals between target service [9]. The use of tantalum also results in lower dose rates due to target activation than silver. However, tantalum suffers from low thermal conductivity, high cost, and is difficult to machine. The low thermal conductivity of tantalum (57 W/m K) has limited previous tantalum targets to operation at or below 1 kW

[10], however cooling geometry designs which minimize conduction distance can largely eliminate the thermal resistance due to low thermal conductivity [2,3]. Thermal modeling of thermosyphon targets has allowed for design optimization of the cooling systems, and tantalum thermosyphon targets have been successfully operated in excess of 2 kW [11]. Aluminum is unsuitable for the target chamber of a production target because it traps fluorine, but it makes an effective test target to observe thermal performance due to its low cost and ease of machining. Aluminum, silver, and tantalum targets were used to validate the computer model.

Target Thermal Model

Thermosyphon targets are pressurized from the bottom via an external expansion volume, and the target chamber is flush with liquid water at the beginning of irradiation. As a result, there is no formation of a distinct vapor region in the top of the target, and boiling characteristics in the target can be adequately modeled by assuming a uniform distribution of void in the target fluid during irradiation.

Heat conduction and convection in a batch boiling target can be modeled using known temperatures and standard heat transfer coefficients. Correlations for boiling and condensing heat transfer coefficients, submerged jets, and coolant flow in channels are widely available in literature. A FORTRAN code was developed to evaluate heat transfer coefficients based on boiling conditions in the target chamber, target pressurization, and coolant flow rates. COMSOL Multiphysics, a program which uses finite element techniques to solve partial differential equations to simulate physical phenomena, was used to solve the heat conduction problem in the target body using the provided heat transfer coefficients and known boundary conditions. Flow circuit models were developed to estimate target cooling water flow based upon the facility's available cooling water supply. Both parallel and serial configurations of the cooling water flow to the back jet and radial cooling channels have been incorporated into the model.

A heat transfer coefficient for single phase forced convection in the radial coolant channels, h_l, can be estimated using the Dittus-Boelter equation for fully developed turbulent flow in smooth conduits or annuli,

$$h_l = 0.023 \frac{k_l}{D} \left(\frac{\rho_l v_l D}{\mu_l} \right)^{0.8} \left(\mathrm{Pr}_l \right)^{0.4}$$

where k_l is the liquid thermal conductivity, μ_l is the liquid dynamic viscosity, v_l is the liquid velocity, D is the diameter of a coolant channel, and Pr_l is the liquid Prandlt number [12].

A heat transfer coefficient for the submerged jet, h_2, can be estimated as

$$h_2 = \frac{k_l}{D} \frac{\left[2 - 4.4\frac{d}{D}\right]}{\left[1 + 0.2\left(\frac{S}{d} - 6\right)\left(\frac{d}{D}\right)\right]} 2\left(\mathrm{Re}_d\right)^{0.5} \left[1 + \frac{\mathrm{Re}_d{}^{0.55}}{200}\right]^{0.5} \left(\mathrm{Pr}_l\right)^{0.42}$$

where d is the jet exit diameter, D is the diameter of the impingement surface, S is the jet exit-to-impingement distance, and Re_d is the Reynolds number with characteristic length d [13].

A heat transfer coefficient for the inside surface of the target chamber, h_b, can be estimated using a correlation for volumetrically heated pools,

$$h_b = \frac{k_l}{H} Nu$$

where H is the height of the target chamber and Nu is the Nusselt number. A correlation for the Nusselt number is given by

$$Nu = \begin{cases} 1.54 Ra^{1/4} & Ra \le 1.865 \cdot 10^{11} \\ 0.0314 Ra^{0.4} & Ra > 1.865 \cdot 10^{11} \end{cases}$$

where Ra is the Rayleigh number. The Rayleigh number is defined to be

$$Ra \equiv \frac{g\alpha H^3 \mathrm{Pr}_l}{\upsilon_l{}^2}$$

where g is the acceleration due to gravity, α is the total void fraction in the target chamber, and υ_l is the liquid kinematic viscosity.

The radial and jet coolant water provided by the facility is typically around 60°F, and the target water is assumed to be at the saturation temperature for the operating pressure. Radial temperature profiles for WMC-1 and WMC-2, generated using COMSOL Multiphysics, are shown in Figs. 3 and 4.

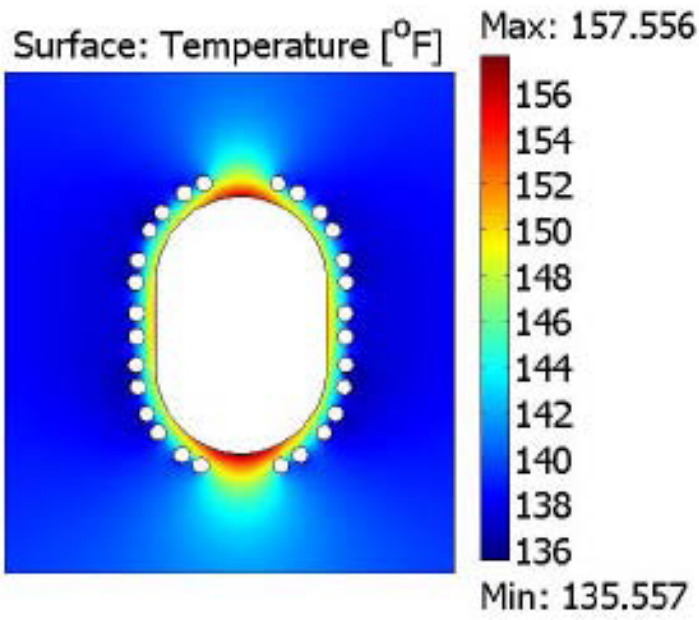

Figrue 3. COMSOL temperature profile for WMC-1 at 400 psi operating pressure and 25% void fraction, corresponding to 1590 W power level.

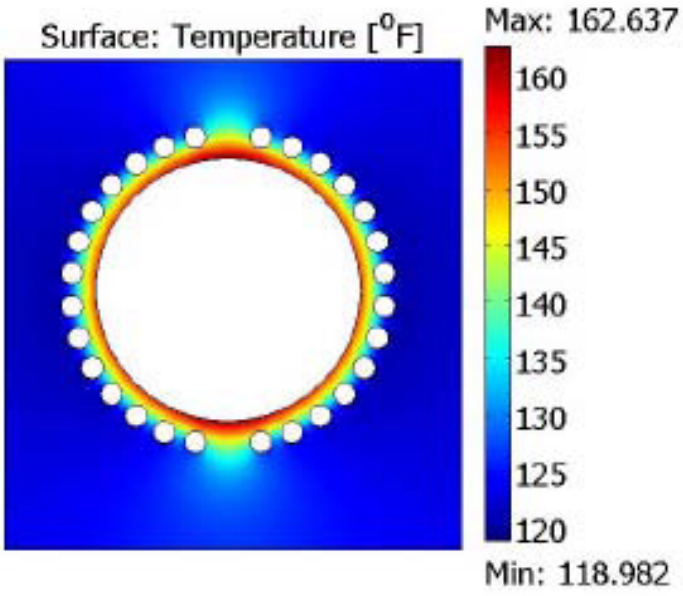

Figure 4. COMSOL temperature profile for WMC-2 at 400 psi operating pressure and 25% void fraction, corresponding to 1730 W power level.

Experimental Validation

Thermosyphon targets have been tested at both the Duke University CS-30 cyclotron and the Wisconsin Medical Cyclotron. The Duke University cyclotron delivers incident proton energy of 22-26 MeV, depending on the attenuator used, and can provide up to 45 μA of beam current. Experimental tests have shown that the Duke University beam shape at the surface of the window foil is irregularly shaped with a maximum diameter of 10 mm. The Wisconsin Medical Cyclotron delivers incident proton energy of 16.5 MeV and can provide a maximum of 100 μA of beam current in standard mode and 150 μA in manual mode. The Wisconsin beam shape at the surface of the window foil has been observed experimentally and can be approximated as roughly circular with a diameter of 13 mm.

During performance tests, the external expansion volume is replaced with a vertical sight tube, which allows for visual observation and recording of displaced liquid volume from the target. Sight tube data was collected over the full range of available beam current for each target described in Table 1. During operation at constant beam power, the displaced water volume in the sight tube was observed to oscillate between a minimum and maximum value as a result of pressure oscillations in the target chamber due to bubble formation and collapse. The minimum and maximum displacement observed at each beam power was recorded and compared to values predicted using the thermosyphon computer model for each target.

Good agreement between model predictions of average target void as a function of beam power and experimental data was observed for four targets which featured different target chamber materials, chamber dimensions, and coolant geometries. The initial onset of boiling can be estimated from the experimental data by observing when small oscillations initiate in the displaced water volume in the sight tube. For all four targets, experimental boiling onset occurs at a lower volume displacement than is predicted for the full thermal expansion process. This suggests that there is subcooled boiling off of the window for average target chamber temperatures below the saturation temperature. The computer model assumes uniformly-distributed boiling initiates in the target following the thermal expansion period, and thus it cannot predict the subcooled boiling which is observed. Consequently, there are discrepancies between the model predictions and experimental data at very low values of average void. When the displaced volume exceeds the level associated with full thermal expansion, there is a distinct increase in the slope of the displacement level with respect to heat input for all cases, which suggests that the target chamber volume has reached saturation.

In Figs. 5-8, the dashed horizontal line represents the point at which small oscillations in the displaced water level indicate subcooled boiling off of the window. The solid horizontal line, at zero void fraction, corresponds to the total water volume displaced into the expansion tube due to thermal expansion of the target water as it is heated from 70°F to the saturation temperature. In Fig. 5, a change in the slope of the upper displacement level which occurs at high beam power for the silver WMC-1 target is most likely due to the onset of beam penetration.

The WMC-2 cylindrical target was installed with parallel cooling circuits from the cooling water supply to the radial cooling channels and the back jet. In this configuration, the cooling water supply manifold was incapable of adequately supplying both cooling circuits, such that the radial cooling channels were starved for flow and heat transfer was dominated by that through the back chamber wall. This significantly alters the vapor distribution in the target and accounts for the greater scatter in the sight tube data, shown in Fig. 6. A serial cooling water configuration is currently planned for testing and should significantly increase the capacity and performance of the target.

Under normal operating conditions, both Duke targets were able to remove the heat generated by the beam with no indication of beam penetration. Sight tube level fluctuations were relatively small and little information could be obtained concerning the model's ability to predict conditions near the target thermal limit. In an attempt to observe target operation approaching the target thermal limit, experiments were conducted at reduced pressure and under conditions of reduced coolant flow. These results are shown in Figs. 7 and 8 respectively. The dramatic swings in sight tube level at the higher power levels are indicative of beam penetration to the back of the target.

Boiling Mode

Good agreement has been observed between model predictions and experimental observations for a model which assumes bulk boiling with no vertical stratification. A model which assumes vertical stratification was also examined, but it failed to accurately predict boiling conditions observed over the range of experimental data. In Fig. 9, observed target void fractions for the silver target WMC-1 are compared to predictions generated by the two models. The vertical stratification model is employed twice, assuming heat transfer in the vapor region is governed by the correlation for either film condensation on a vertical plate (Vertical Plate) or laminar condensation within a horizontal tube (Horizontal Tube). When the target chamber becomes fully saturated, the bulk boiling model accurately predicts average target void fraction over the range of experimental data. The vertical stratification model, using either condensing heat transfer condition, does not adequately predict target behavior.

Conclusions

Computational models have been developed for the design and optimization of boiling batch production targets. Good agreement has been observed between model predictions of average target void as a function of beam power and experimental measurements from the Duke University Medical Cyclotron and the Wisconsin Medical Cyclotron. Development of an accurate computer model to predict target thermal performance has fundamentally changed the target design process, and has led to the design of new targets with enhanced production capabilities. Tantalum production targets are currently in operation at both the Duke University Medical Cyclotron and the Wisconsin Medical Cyclotron. These targets have been shown to operate consistently at beam powers in excess of 1 kW with high ^{18}F yields [11].

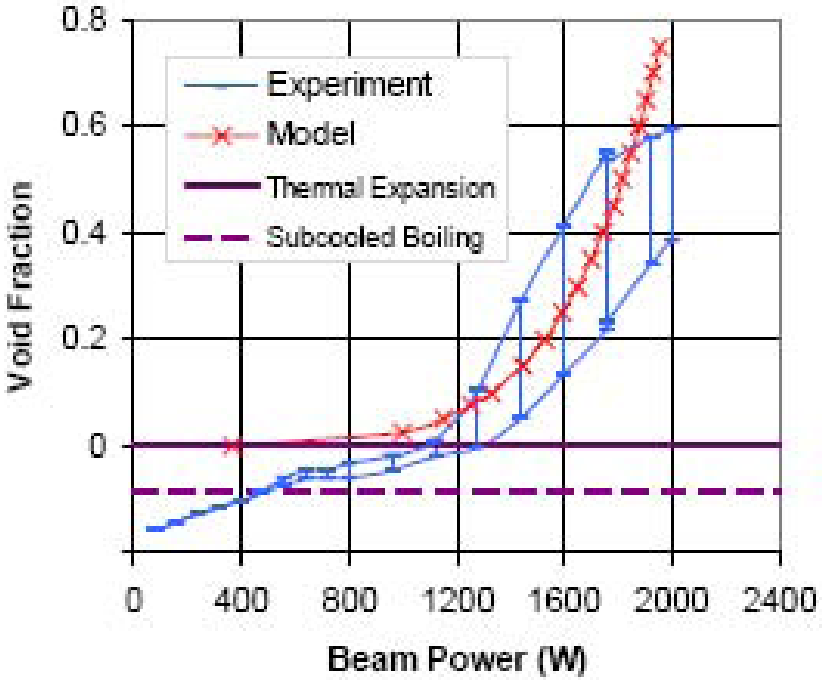

Figure 5. Target void fraction versus beam power for WMC-1 at 400 psi operating pressure.

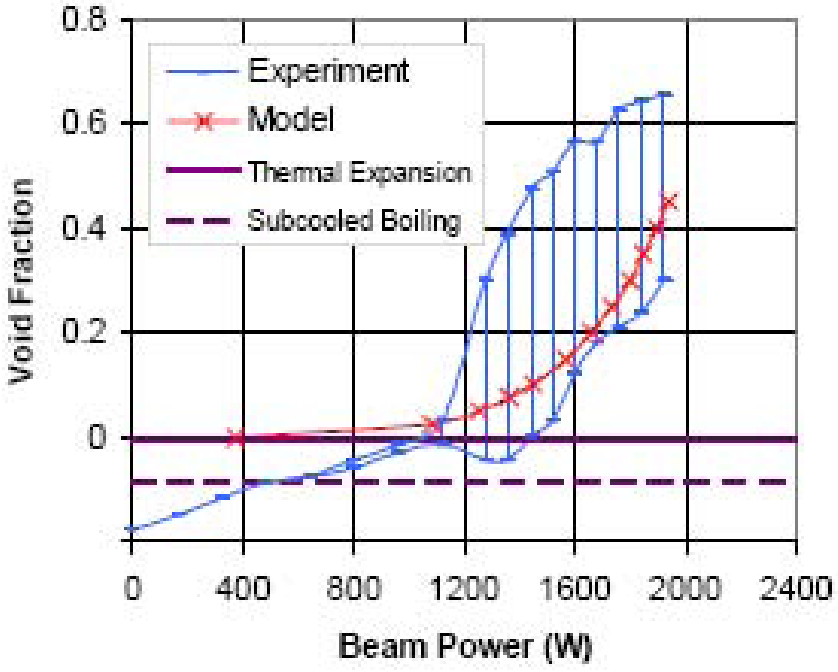

Figure 6. Target void fraction versus beam power for WMC-2 at 425 psi operating pressure.

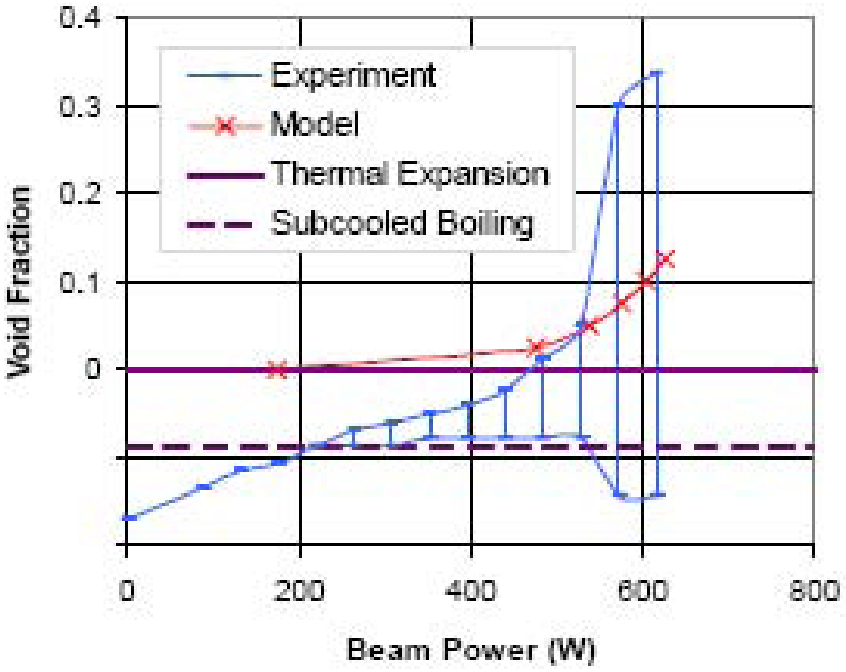

Figure 7. Target void fraction versus beam power for DUKE-1 at 200 psi operating pressure.

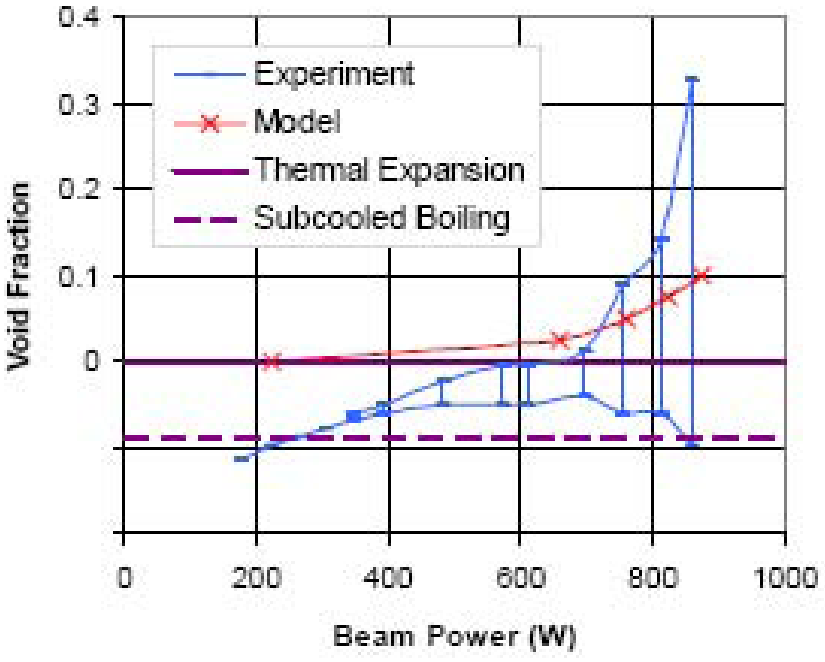

Figure 8. Target void fraction versus beam power for DUKE-2 at 400 psi operating pressure.

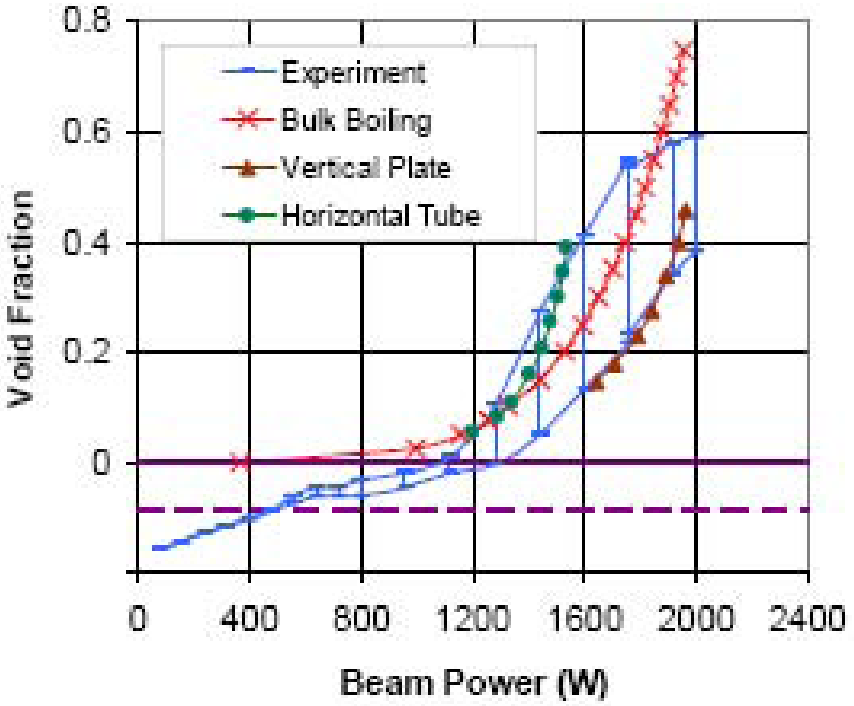

Figure 9. Comparison of target void fraction versus beam power for WMC-1 at 400 psi operating pressure to bulk boiling and vertical stratification models.

References

[1] J. Cornelius, M. Humphrey, M. Doster and B. Wieland, Finite Element Modeling of Thermosyphon Batch Targets, Targetry and Target Chemistry: 11th Int. Workshop, Cambridge, 2006.

[2] J. Peeples, Design and Optimization of Thermosyphon Batch Targets for Production of ^{18}F, Master of Science Thesis, Department of Nuclear Engineering, North Carolina State University, North Carolina, 2006.

[3] J. Peeples, Design and Testing of Thermosyphon Batch Targets for Production of ^{18}F, PhD Thesis, Department of Nuclear Engineering, North Carolina State University, North Carolina, 2008.

[4] J. Peeples, M. Stokely and M. Doster, Development and Validation of Computer Models for Design of Batch Boiling Targets for Production of ^{18}F, Targetry and Target Chemistry: 12th Int. Workshop, Washington, 2008.

[5] A.E. Ruggles, C.W. Alvord, in: J.L. Duggan, I.L. Morgan (Eds.), CP576, Application of Accelerators in Research and Industry: 16th Int. Conference, AIP Press, 2001, p. 817.

[6] J.G. Collier, Convective Boiling and Condensation, McGraw Hill, UK, 1981.

[7] M. Stokely, Advanced Thermosyphon Targets for Production of the ^{18}F Radionuclide, Master of Science Thesis, North Carolina State University, North Carolina, 2007.

[8] K. Quinn (Ed.), Havar Technical Data Sheet, Hamilton Precision Metals, Pennsylvania.
[9] N. Satyamurthy, B. Amerasekera, C.W. Alvord, J.R. Barrio and M.E. Phelps, Tantalum [18O]Water Target for the Production of [18F]Fluoride with High Reactivity for the Preparation of 2-Deoxy-2-[18F]Fluoro-D-Glucose, *Molecular Imaging and Biology* **4** (2002), pp. 65-70.
[10] C.W. Alvord, A.C. Williamson, T.L. Graves and S.S. Zigler, Design, test and widespread implementation of a compact kilo-Watt fluoride ion target, *Nucl. Instrum. Methods Phys. Res. B* **241** (2005), pp. 708–712.
[11] M. Stokely, Testing and Analysis of Advanced Thermosyphon Target Systems for Production of Aqueous [^{18}F]Fluoride via ^{18}O(p,n) ^{18}F, PhD Thesis, Department of Nuclear Engineering, North Carolina State University, North Carolina, 2008.
[12] F.P. Incropera, D.P. Dewitt, T.L. Bergman and A.S. Lavine, Introduction to Heat Transfer, Fifth Edition, John Wiley & Sons, New York, 2007.
[13] H. Martin, Heat and Mass Transfer Between Impinging Gas Jets and Solid Surfaces, *Advances in Heat Transfer* **13 (**1977), pp.1-60.

Recirculating Targets for ^{18}F Radionuclide Production

Abstract

Flourine-18 is commonly produced through proton irradiation of ^{18}O enriched water by the $^{18}O(p,n)^{18}F$ reaction. Heat deposited in the target fluid by the proton beam is proportional to the ^{18}F produced, thus production is often limited by the targets ability to reject heat. For power levels above 3 kW, boiling batch targets with local cooling can become impractical due to excessive ^{18}O water volumes. One potential solution is a recirculating target system where the target water velocity is sufficient to prevent boiling. In this design the heated fluid travels through an external heat exchanger of sufficient capacity to remove the heat, and then through a pump which returns the cooled fluid to the target. A high-flow/low-volume pump and a high-capacity/low-volume heat exchanger are essential to the overall performance of the recirculating target. In this work, two different types of heat exchangers are considered. Laboratory testing was conducted on a small shell and tube heat exchanger that removed nearly 6 kW of heat at flows provided by a miniature regenerative turbine pump. Laboratory testing was also conducted on a small cross flow heat exchanger with measured performance of 7.4 kW and predicted peak performance approaching 10 kW.

Introduction

The recirculating target is one design under consideration for the production of the ^{18}F radionuclide. Common to all ^{18}F water targets, large amounts of waste heat is deposited in the target fluid during operation. Therefore, a common problem for all designs is effective target cooling. A recirculating target pumps the heated fluid to an external heat exchanger where the heat is transferred to a low temperature heat sink. A typical design constraint for recirculating targets is that the target water remains below the boiling point at all times. Figure 1 shows the general layout of the recirculating target system.

A first generation recirculating target design incorporated a two-pass, plate-type heat exchanger as the primary heat sink [1]. This heat exchanger had multi pass flow channels with the intent of increasing surface area and heat transfer efficiency. The heat exchanger was tested at heat transfer rates up to 4.5 kW, but weighed in excess of 20 pounds and had an internal target water volume of 17 mL. It was discovered that this heat exchanger had misaligned plates that reduced its effectiveness. Even so, the design still fell short of the overall goals of the recirculating target system. When considering weight alone, this design was by no means compact. The design goals for the recirculating target are heat transfer rates in excess of 10 kW with minimum weight and volume. It is unlikely that the two pass plate-type heat exchanger has the necessary capacity, or can be easily implemented in a recirculating target system. Figure 2 shows a picture of the first generation plate-type heat exchanger. [1]

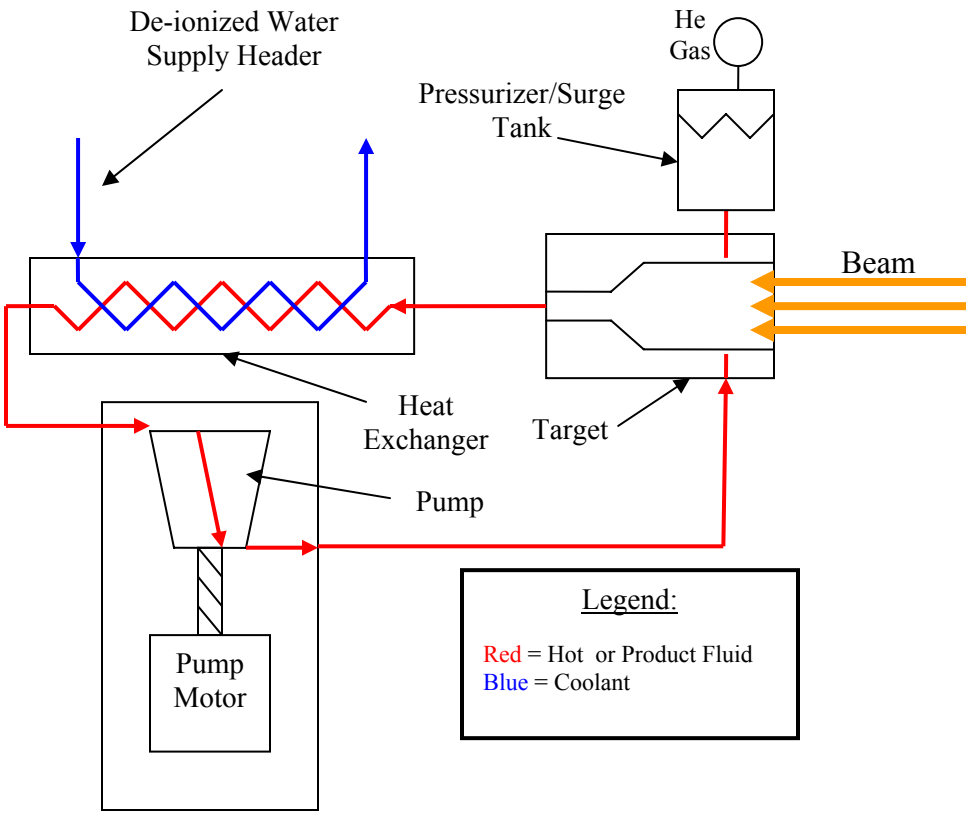

Figure 1: General layout of recirculating target system

Figure 2: First generation two pass plate-type heat exchanger [1]

New designs are required to expand the options available for providing efficient, compact, and high capacity heat removal for the recirculating target system. Three goals are essential to the success of a new heat exchanger design. These goals include: having a small primary or "product" side volume, physical dimensions that allow for easy implementation into an integrated target design, and a heat removal rate of 10 kW. Two competing heat exchanger designs are considered in this work, a counter flow shell and tube heat exchanger, and a compact cross flow heat exchanger. The specific aims of this research are:

- Design, optimize and test a compact shell and tube heat exchanger compatible with the regenerative turbine pump and the integrated recirculating target system
- Design, optimize and test a compact cross flow heat exchanger compatible with the regenerative turbine pump and the integrated recirculating target system
- Simulate the performance of the integrated recirculating target system with the selected heat exchanger under different operating conditions and heat loads

Cross flow heat exchangers are more commonly used for compact designs, whereas shell and tube heat exchangers are commonly found in larger more robust applications such as cooling industrial machinery oils. Shell and tube heat exchangers are suitable for this application because they are easily implemented into industrial settings, and are relatively cheap to construct and repair. This study discusses the design, simulation, and selection of both types of heat exchangers.

Compact Shell and Tube Heat Exchanger

A shell and tube heat exchanger is comprised of a large outer shell (typically cylindrical) with a series of staggered or in-lined tubes inside the shell. One fluid flows within the tubes, while the second fluid flows through the shell over the outside of the tube bundle. In practice, the hot or cold fluid can be contained in either the inside or the outside of the tubes. For example, in a steam condenser the cold fluid flows on the inside of the tubes and the steam is allowed to pass over the tubes and condense. Alternately, the hot fluid can flow on the inside of the tubes and the cold fluid can flow on the outside as with industrial oil coolers. [5, 6]

After setting which side of the heat exchanger will be the primary side (the hot fluid) and the secondary side (the cold fluid), it is necessary to select either a counter or parallel flow configuration. In counter flow heat exchangers, the primary and secondary sides flow in opposite directions, whereas in parallel flow heat exchangers both sides flow in the same direction. Counter flow promotes a higher log mean temperature difference between the primary and secondary side, thus promoting more efficient heat transfer. Using counter flow typically reduces necessary area and/or flow velocity required to produce a desired heat transfer rate. As a result, counter flow designs are the most commonly used. Figure 3 shows the flow paths in a typical counter flow shell and tube heat exchanger.

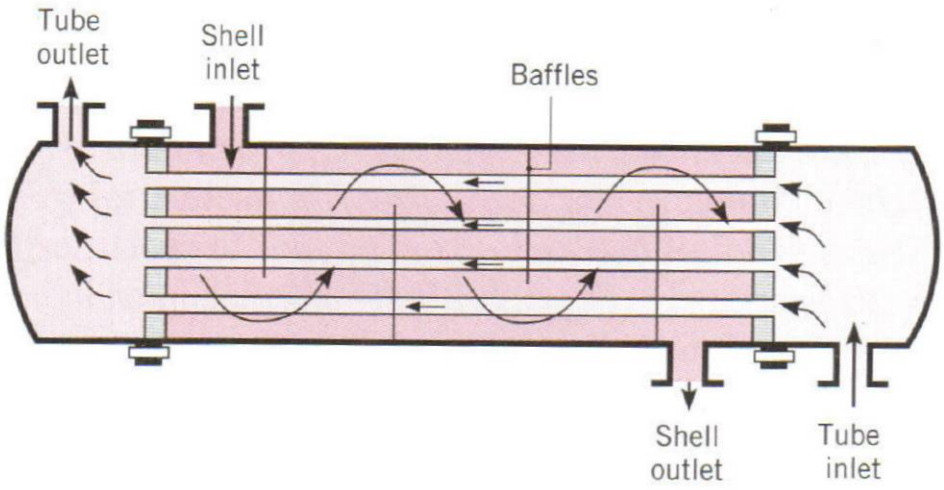

Figure 3: General operation of a counter flow shell and tube heat exchanger [6]

A shell and tube heat exchanger is an ideal design for this study. By setting the inside of the tubes as the primary side, it is possible to maintain a small product volume. The primary side or product side fluid is expensive (typically $50/mL) and consists of enriched ^{18}O water. It is desirable to keep this volume as small as possible in the event of spills or contamination and to maintain a minimum inventory. The volume on the shell side is typically larger by design and in comparison to the tube side will easily accommodate high flows. Because the coolant flow available for the recirculating target system is much larger than the necessary primary flow, it makes sense to use the shell side of the heat exchanger for cooling. Furthermore, the actual dimensions of a shell and tube heat exchanger vary widely depending on the numbers of tubes, tube diameters, and tube lengths. Different component dimensions can be evaluated based upon their performance and compatibility with regards to the integrated recirculating target. In summary, a shell and tube heat exchanger is an extremely versatile platform for compact designs.

Regenerative Pump

A prototype regenerative turbine pump had been selected for the integrated recirculating target and served as the basis for a feasibility study of the recirculating target design [1]. The current pump incorporates a horizontal shaft with two seals and two bearings on the shaft. The impeller and shaft are made of stainless steel. The impeller uses opposing double rows of vanes that produce screw-type fluid flow through the body of the pump. As the impeller rotates the pressure increases in a series of small pressure impulses. Because fluid pressure is gradually increased the effects of collapsing bubbles in a two phase mixture are greatly reduced. The added versatility of being able to run two phase mixtures is necessary in the event that localized boiling occurs in the system and the mixture is transported through the pump before condensing. [9]

Modifications to the regenerative turbine pump included a change in the main drive. The current shaft driven design couples the pump impeller directly to the electric driving motor. This design requires shaft seals that are prone to failure after extended use. To eliminate the shaft seals, a magnetic drive was designed that eliminates direct coupling between the pump and the driving motor. Studies were also performed to optimize the size, dimensions and orientation of the impeller to maximize performance at moderate pump speeds. The magnetic drive failed to provide sufficient torque to generate the flows necessary for power demands of interest to this work. Similarly variations in impeller design failed to produce pumps with significantly different performance than the original pump design. As a result, the results presented here were all obtained with the base pump design. General dimensions of the current pump base are 5.03 cm high, 5.03 cm deep, and 3.18 cm long with an impeller diameter of 2.79 cm. The impeller has 20 notches, thus 20 vanes on each side. Figure 4 shows the general layout and assembly of the regenerative turbine pump and impeller. [1]

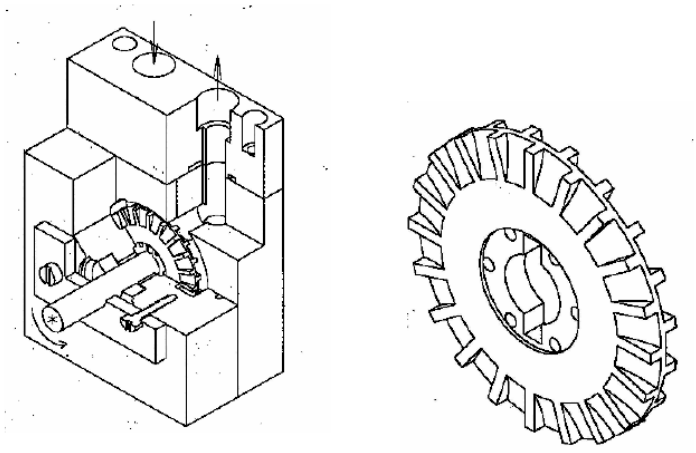

Figure 4: Regenerative turbine pump assembly and impeller [1]

The performance characteristics of the regenerative turbine pump consist of a correlated equation in terms of pump speed, volumetric flow rate, and pressure drop across the pump. This correlation is assumed accurate for use in this research and supplies the basis for establishing a reasonable range of flow rates and pressure drops for the integrated recirculating target design. [1]

$$\Delta P_p = a_0 + a_1\Omega + a_2\Omega^2 + a_3 G + a_4 G^2$$

This correlation allows the differential pressure across the pump to be calculated for any flow rate at a given pump speed. The pressure drop across the pump is set by the rest of the flow system which could include the heat exchanger, connecting tubing, the target, and the pressurizer.

Prototype Tube and Shell Heat Exchanger

Computational models were developed to simulate the performance of compact tube and shell heat exchangers and optimization studies performed to select potential designs for a prototype. [3] The design study identified heat exchanger characteristics

such as tube quantity, tube diameter and length, the shell diameter, and even the materials to be used.

Contracting with either the NCSU or Duke Medical Center machine shops to fabricate the prototype heat exchanger was considered. While the shell of the heat exchanger is simple to construct, construction of the tube bundle requires aligning and inserting baffles and is significantly more involved. If finned tubes are used, this process would be even more complicated. In addition, it would be difficult to attach thin wall tubes to the bulk heads of the heat exchanger. Brazing thin tubes in the arrangement required is problematic and requires specialized furnaces, materials, and experience. Furthermore, the availability of suitable tubing sizes could reduce the overall effectiveness of the proposed designs.

Insuring a sealed boundary at the inlet and outlet points of the primary side that will reliably separate the primary and secondary sides is difficult on this size scale. If this cannot be performed correctly, the heat exchanger will not function properly. Based on these considerations, it was decided to seek out an established shell and tube heat exchanger manufacturer to build the prototype.

Exergy, LLC specializes in the design and construction of compact shell and tube heat exchangers. They have over ten different standard off-the-shelf designs that can be purchased. Of interest to this work are their 10 series, shell and tube heat exchangers. The 10 Series incorporates Exergy's smallest tube sizes of 0.094" OD with 0.010" wall thickness. This series has a general shell ID of 10 mm. All tube bundles consist of 7 staggered smooth tubes. The difference between the models in the 10 series shell and tube heat exchangers are the tube lengths. Tube lengths offered include 4, 8, and 12". Their corresponding primary side volumes are approximately 2, 4, and 6 mL. [4]

The Exergy 10 Series shell and tube heat exchangers are similar in size and configuration to several of the designs identified in the optimization study. Both heat exchanger designs use an array of 7 staggered smooth tubes. The smallest of the 10 Series heat exchangers has a tube length of 10.2 cm which is slightly shorter than the design length of 12 cm. Tube ID for the optimized design was set to be 2.4 mm whereas the 10 Series heat exchangers use 1.9 mm tubes. Shell diameters for both are around 10 to 12 mm. Tube pitch for the optimized design was 3.64 mm and for the 10 Series is 3.00 mm, both of which are 25% larger than the tube OD. All 10 series shell and tube heat exchangers are made of 316 SS. Stainless steel is desirable for durability, longevity, and can be used with radiopharmaceuticals.

Due to its versatility, the model 00268-2 heat exchanger was selected for the prototype shell and tube heat exchanger. Figure 5 shows a picture of the Exergy LLC model 00268-2 shell and tube heat exchanger beside a standard writing pen.

Figure 5: Exergy LLC model 00268-2 shell and tube heat exchanger

Manifolds for the 10 Series heat exchangers are simple pipe fittings. The calculated volume per manifold for the model 00268-2 heat exchanger is ≈ 0.4 mL.

To reduce the risk of cracking, Exergy imposes a limit on the maximum average temperature difference (MATD) its heat exchangers should experience during operation. The MATD is defined to be the difference between the averages of the primary and secondary side inlet and outlet fluid temperatures. [4]

$$MATD = \left(\frac{T_{h,i} + T_{h,o}}{2} \right) - \left(\frac{T_{c,i} + T_{c,o}}{2} \right)$$

Exergy recommends the MATD should not exceed 125 °F. This MATD value is somewhat conservative and limits the overall performance of the heat exchanger. However, even with this limit Exergy predicts around 4.2 kW for their smallest heat exchanger at the expected flow rates of the integrated target system.

Experimental Tests

Bench top experiments were performed on the Exergy model 00268-2 heat exchanger to validate the simulation results. The original regenerative turbine pump was used to drive the primary side of the heat exchanger. This pump was designed to supply high pressure head and flow rates with minimal internal volume. The measured pump performance curves were also used as a basis for the simulated results. For the secondary side, the building water supply stepped up by a 0.5 hp FLOTEC utility pump was used to simulate expected supply pressures from a test facility de-ionized water supply. Secondary water conditions were held constant with a supply pressure of 62 psig and a

temperature of 80 °F. The heat source came from an adjustable 0 to 9 kW WATLOW circulation heater. The primary side flow rate was recorded by a calibrated 0 to 3 psi Rosemont ΔP pressure transducer. A ΔP vs. Flow rate correlation was also established for the secondary side of the Exergy heat exchanger that was then used to calculate the heat transfer rate for the secondary side [3].

Independent tests were conducted to gather the pressure drop vs. flow data. An Omega 0 to 75 psi ΔP pressure transducer was used to record pressure drops and a Rosemont 0 to 3 psi ΔP pressure transducer was used to record flow rates. Automated data collection was performed using LabVIEW and a series of Field point modules. LabVIEW was able to record all necessary temperatures and pressures throughout the system.

Data gathered from the experiments were compared to the theoretical models. Of interests is heat transfer vs. primary side flow rate. Figure 6 displays the thermal performance data.

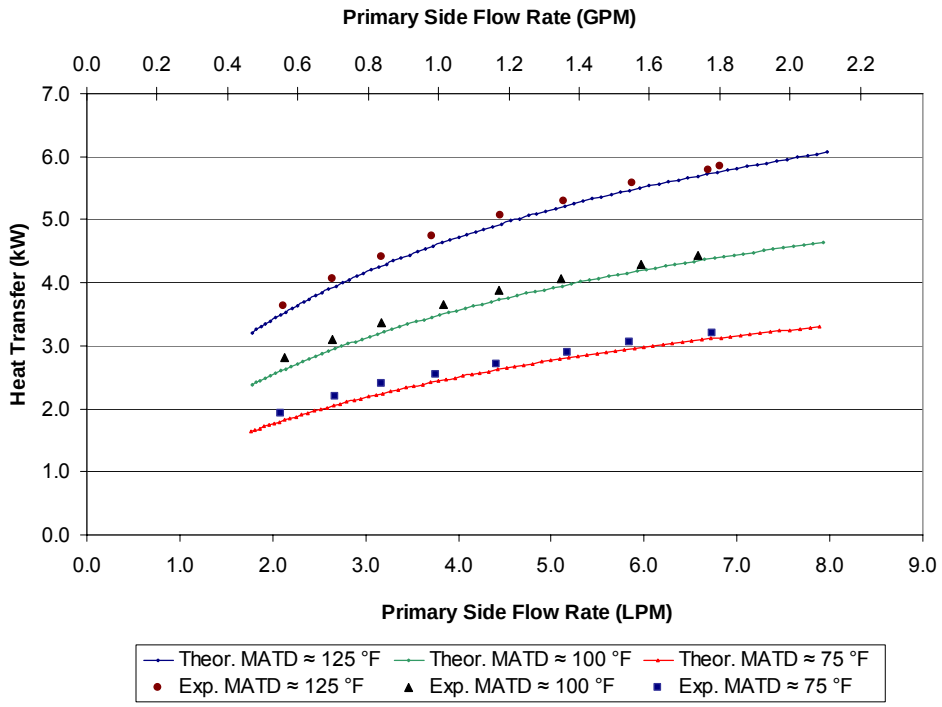

Figure 6: Exergy model 00268-2 thermal performance results

From Figure 6 it can be seen that the experimental data match the simulation results well for all three test Mean Average Temperature Difference (MATD) levels. Because the slope of the simulation and experimental data are close to the same, it appears that the primary side model is accurately predicting heat transfer as the primary side flow rate increases. Therefore, the difference between the simulated and measured results is likely due to under predicting the secondary side thermal performance. This is possibly due to minor dimensional discrepancies between the actual tube pitch and what

was measured directly from the heat exchanger. Exact tube pitch dimensions were not attainable due to their proprietary nature.

It should also be noted that variations in the slope of the experimental data is most likely due to inadequacies with the regenerative turbine pump. Throughout the tests variations in pump speed caused ± 0.024 LPM fluctuations in primary side flow rate. This is because of the type of electrical motor that is used for the first generation regenerative turbine pump.

The experimental results have shown the simulation models are capable of simulating the thermal performance of the combined heat exchanger and regenerative turbine pump. It should also be noted that the simulation and experimental results show a strong relation between primary side flow rate and heat transfer rate. This is because the majority of the thermal resistance is in the primary side heat transfer coefficient. These results imply performance of the integrated target system can be improved if a higher capacity pump can be developed.

Compact Cross Flow Heat Exchanger

A cross flow heat exchanger refers to designs in which the hot and cold fluids are passed perpendicular to one another without making physical contact. Heat is conducted through a media between the two fluids. In order to maximize the performance of a cross flow heat exchanger the wall resistance must be minimized by using extremely thin walled channels. Minimizing the conduction resistance also makes the heat exchanger performance independent of the conduction material. Increased performance is also obtained by maximizing the convective properties of a high flow, low temperature secondary side.

Cross flow heat exchanger designs include flow between two flat plates, while other designs use molded rectangular or bored circular channels. Many cross flow heat exchangers have nearly identical primary and secondary side geometries, therefore they operate well in situations where the primary and secondary side flow characteristics are similar with a high temperature difference between sides, yet still benefit if the secondary side has larger flow rates as this will minimize heat transfer resistance on the secondary side. By minimizing wall resistance cross flow heat exchangers are very efficient and are a strong choice for use in compact designs. [7]

A common characteristic among cross flow heat exchangers is the intricate flow paths used to increase heat transfer. As stated above, most flow paths are contained between two plates, or a series of channels perpendicular to one another. Designing a series of individual channels increases heat transfer surface area. Designs exist which incorporate over 3000, 100 - 150 μm square channels on a 1 cm^2 surface [2, 8]. In this configuration the flow is basically passing through a fine screen mesh, where the pressure drops are minimal, the convective heat transfer coefficients are high and wall resistance is at a minimum. Designs such as these are ideal, but extremely difficult and expensive to fabricate. Other, more practical designs such as the use of a series of bored circular

channels are very effective while remaining relatively easy to design and fabricate. Figure 7 shows the general size and shape of a cross flow heat exchanger.

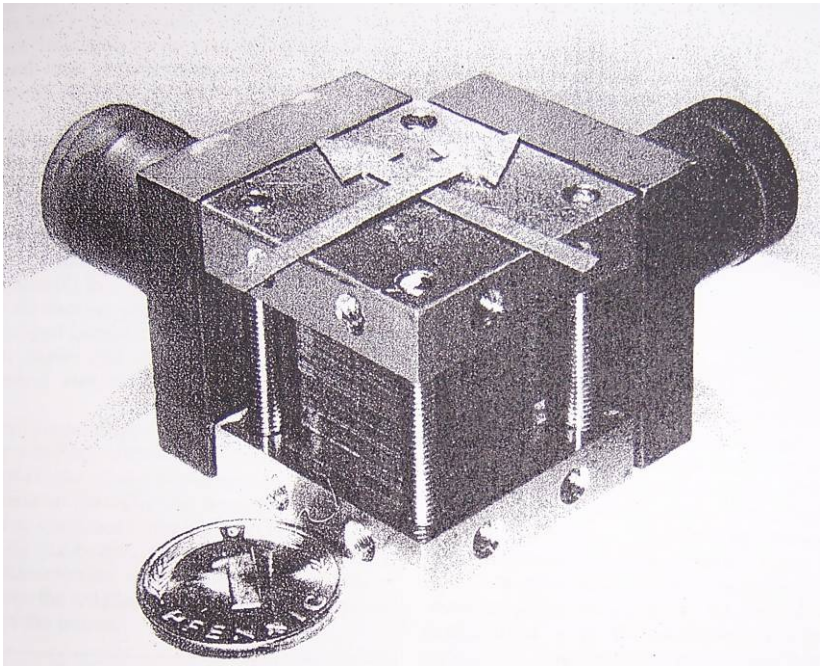

Figure 7: Cross flow heat exchanger [8]

Cross flow heat exchangers are ideal for compact designs. They use small channels and wall thicknesses to maximize heat transfer rates. Furthermore, if constructed as a one-piece part, a cross flow heat exchanger can handle larger thermal stress than other designs. The cross flow designs considered in this study consist of machined and tapped channels in a solid core.

A compact cross flow heat exchanger is another option for use with the integrated recirculating target design. In particular, a solid block cross-flow design is simple and reliable. This design would require a solid piece of metal stock to be shaped into a cube, into which the coolant channels can be bored directly. The material choice for this design will be based on heat transfer rates, machinability, and compatibility with the integrated target design and the production of the ^{18}F radionuclide.

In order to determine an optimal cross flow heat exchanger design, it is necessary to simulate different combinations of channel diameter and length, as well as the wall thickness. Assuming a primary flow rate, pressure drops across the heat exchanger and other devices in the system must be determined. Computational models were developed to predict the performance of the cross flow heat exchanger and optimization studies performed to identify potential prototype designs [3]. A circular channel cross flow heat exchanger was then designed and constructed to validate the computational models. Figure 8 displays a dimensioned drawing for the cross flow heat exchanger. Figures 9 and 10 show two different views of the constructed cross flow heat exchanger.

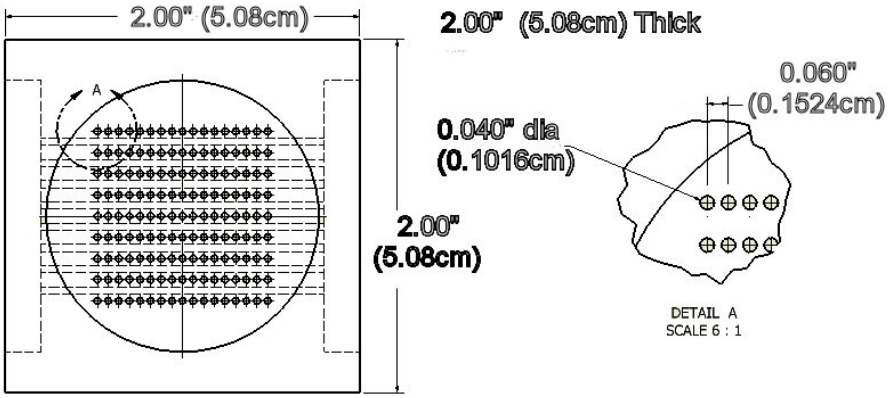

Figure 8: Dimensioned drawing of the cross flow heat exchanger

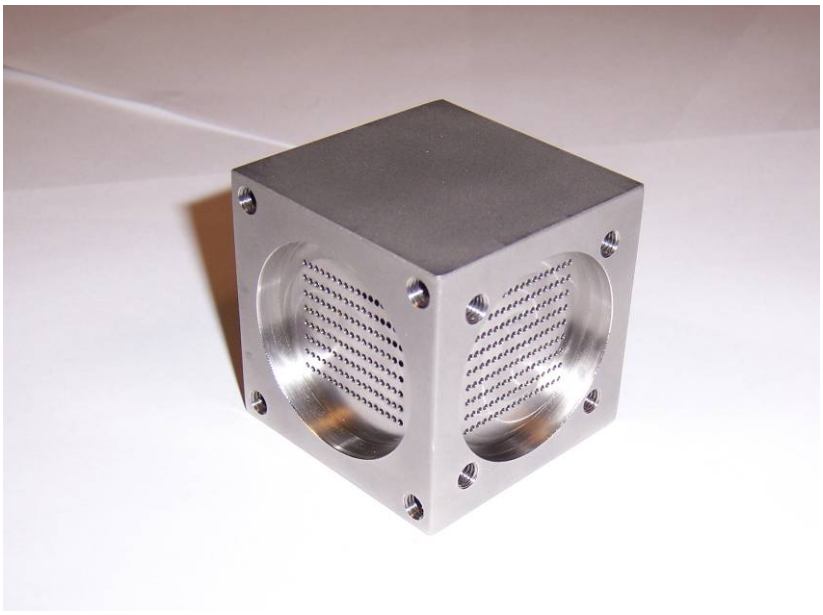

Figure 9: Corner view showing primary and secondary sides

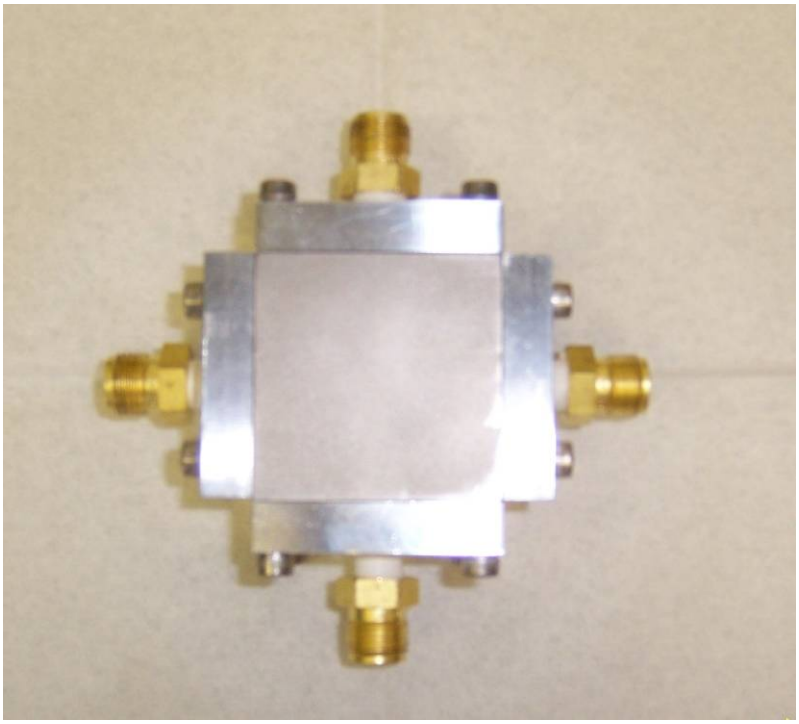

Figure 10: Assembled view with manifolds and fittings attached

Results of Experimental Tests

Experiments were performed to validate the theoretical models of the circular channel cross flow heat exchanger. Of interest is the heat transfer vs. primary side flow rate. Figure 11 displays the thermal performance data. The experimental data match the theoretical simulation results well across all six tested MATD levels. Similar to the testing of the shell and tube heat exchanger, variations in pump speed caused ± 0.024 LPM fluctuations in the primary side flow rate. Also during the testing of the cross flow heat exchanger the pump experienced seal and bearing failures which caused the pump to run with more vibrations. This could have reduced the performance of the pump. It should be noted that the results show a strong relation between primary side flow rate and heat transfer rate. This is because the heat transfer resistance is the highest on the primary side throughout the experimental primary side flow rate span, but reduces as flow rate increases.

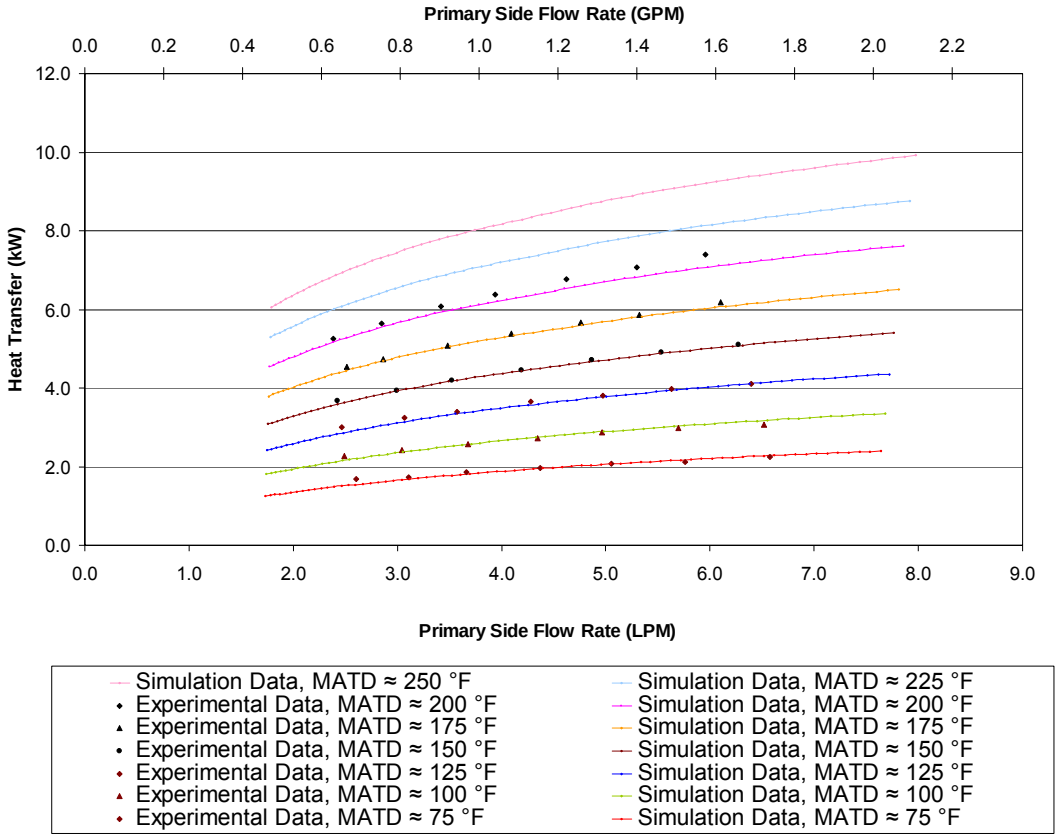

Figure 11: Compact Cross Flow Heat Exchanger Thermal Performance

Integrated System Simulation

Two heat exchangers have been designed, simulated, and experimentally tested. Laboratory experiments show that the models established to simulate the thermal performance of these heat exchangers are accurate, making it possible to simulate the performance of an itegrated recirculating target system. It is also useful to determine if construction of a cross flow heat exchanger with smaller channel diameter and channel spacing would further benefit the integrated recirculating target system performance. The alternate cross flow heat exchanger design has 0.030" diameter channels and 0.010" channel spacing. It is also useful to compare the model 00268-1 shell and tube heat exchanger, the next larger of the Exergy 10 Series.

One major concern for the integrated recirculating system is physical dimensions. The shell and tube heat exchanger has the smallest footprint of the two built designs. It is 4.9 inches long, 0.6 inches wide, 1 inch tall and weighs 0.35 pounds. The Exergy model 00268-1 shell and tube heat exchanger is roughly twice as long and heavy. The cross flow heat exchanger has rough dimensions of 2.5 inches cubed with a weight of around 2 pounds. The alternate design cross flow heat exchanger would have similar physical dimensions. With the manifolds, both built heat exchangers require even more space to

be added to the system. But even with manifolds, the shell and tube heat exchanger is the smallest. Figure 12 shows both heat exchangers with manifolds.

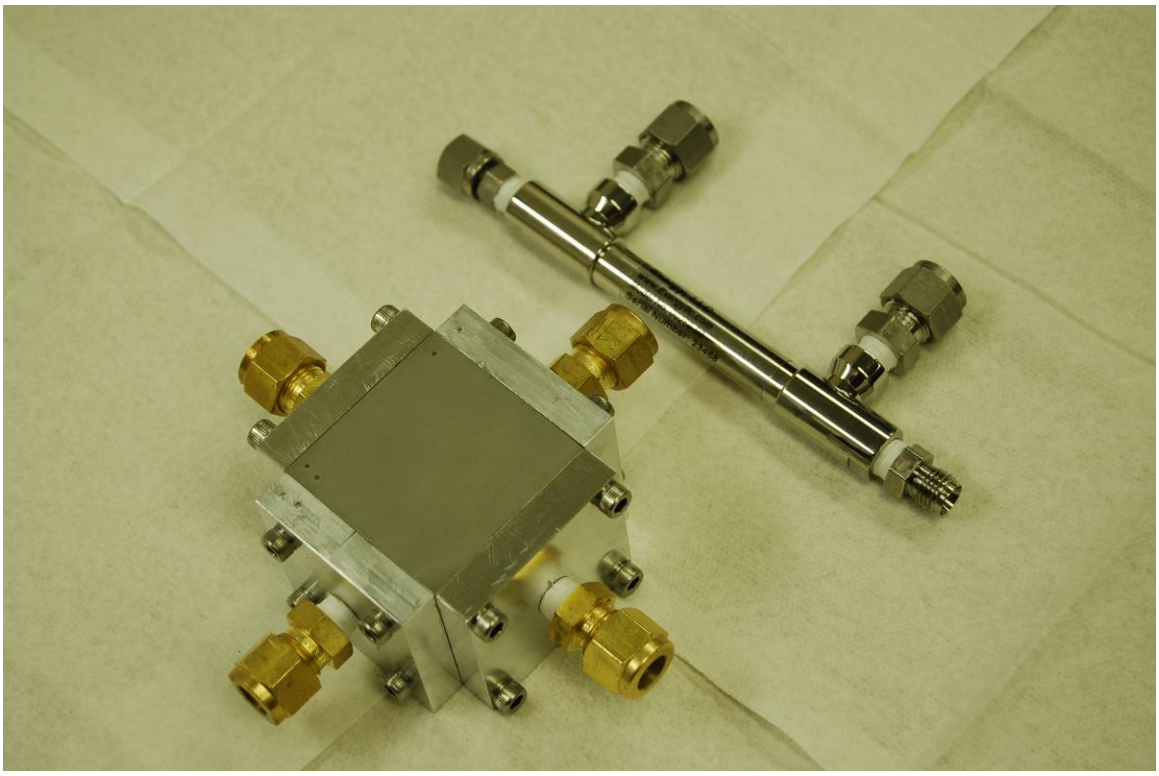

Figure 12: Both heat exchangers with manifolds

It is desirable that the recirculating system operates at the lowest temperature and pressure possible. This minimizes stresses on all components in the system. The operational limits of the shell and tube heat exchanger, primarily the MATD, put it in the desired range for the integrated recirculating system. In order to better compare the cross flow and the shell and tube heat exchangers, the designs should be compared at equivalent levels of exertion. One way to do this is to simulate the performance of the heat exchangers at identical MATD levels. This will cause inlet temperatures to be similar and will give a better comparison of their performance differences. It is also useful to compare the built designs to the alternate cross flow and the Exergy model 00268-1 shell and tube heat exchangers simulated in this study at the same MATD. In the future, these heat exchangers could be built and operated if feasible. Table 1 shows general dimensions, capacities, and performance of both built heat exchangers as well as the alternate cross flow and Exergy model 00268-1 heat exchangers.

Table 1: Comparison of four heat exchanger designs

	Built Prototypes		**Additional Designs**	
	Shell and Tube Model 00268-2	Cross Flow (Design 2)	Shell and Tube Model 00268-1	Alternate Cross Flow
Primary Volume (mL) =	2.01	4.48	4.00	5.56
Manifold Volume (mL) =	0.40	2.00	0.40	2.00
Total Primary Volume (mL) =	2.81	8.48	4.80	9.56
Primary Flow Rate (LPM) =	3.47	3.33	3.46	3.41
Secondary Flow Rate (LPM) =	12.59	12.17	6.66	13.28
	MATD = 125 °F for a pump speed of 5500 RPM			
Heat Transfer (kW) =	4.49	3.26	8.54	5.52
Load Density, *excluding manifold volume* (kW/mL) =	2.23	0.73	2.14	0.99
Load Density, *including manifold volume* (kW/mL) =	1.60	0.38	1.78	0.58
Primary Inlet Temperature (°F) =	231.9	226.6	260.0	237.2

It can be seen that all four heat exchangers have similar values for primary and secondary flow rates. The primary side inlet temperature is strongly dependent upon the heat transfer rate, thus the model 00268-1 shell and tube heat exchanger has the highest primary inlet temperature. The primary side flow rates are similar because the heat exchangers are being simulated in operation with the testing apparatus where the majority of the pressure drop is present in the test equipment rather than the heat exchanger.

There are several differences between the four heat exchangers. The primary side volumes are higher for the cross flow heat exchangers across the board. Not only the actual channels of the cross flow heat exchangers have more volume than the tubes in the shell and tube heat exchangers, the manifolds have a higher volume as well. The volume of one cross flow manifold is equal to the volume of the primary side of the model 00268-2 shell and tube heat exchanger. The cross flow heat exchangers have roughly 300% more primary side volume than the model 0026802 shell and tube heat exchanger when including manifold volumes. As far as heat transfer, the model 00268-2 shell and tube heat exchanger has 31% more capacity that the prototype cross flow heat exchanger and has approximately 1 kW less capacity than the alternate cross flow heat exchanger. When load densities are compared, the shell and tube heat exchangers are proven to be far more efficient than both cross flow heat exchanger designs.

The wall thickness of heat exchangers plays an important part in regulating the heat transfer rate. The wall thickness also sets how much of an affect inputs such as flow rates and inlet temperatures have on the performance of a heat exchanger. Figure 13 shows a thermal performance simulation of the built cross flow and the shell and tube heat exchangers as well as the other two designs under laboratory testing conditions. Notice the difference in slope as well as magnitude throughout the primary side flow rate span.

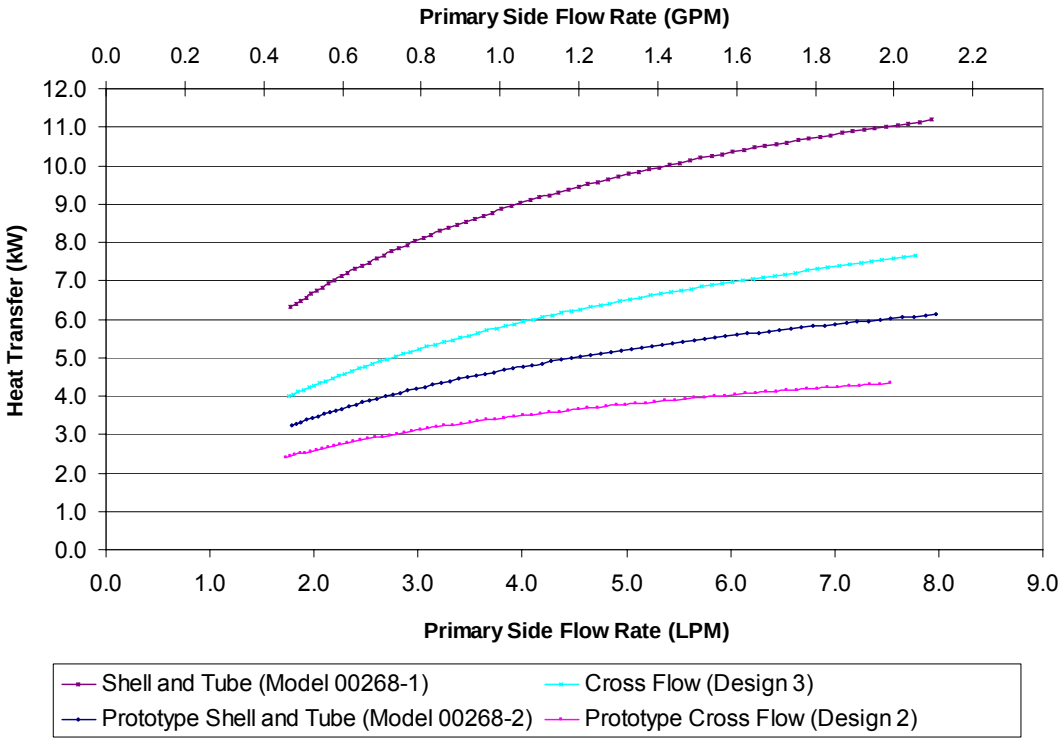

Figure 13: Comparison of built and alternate heat exchanger designs at an MATD of 125 °F

Comparisons of the four heat exchangers at common operational level indicate he shell and tube heat exchangers have advantages in all design categories. In comparison to the built and alternate cross flow heat exchangers the shell and tube heat exchangers have higher heat transfer rate per unit volume. The shell and tube heat exchangers are also less than a quarter of the weight and have a much smaller footprint in the integrated recirculating target system. Even though the cross flow heat exchanger could be revised and a new prototype built, this study indicates that the shell and tube heat exchanger is still the best choice.

The two considered shell and tube heat exchanger designs are essentially the same except that the model 00268-1 is twice as long as the model 00268-2. Because manifolds volume is the same for both models, the volume difference between the models is less than half. When including manifold volume, the model 00268-1 has a higher load density than the model 00268-2 heat exchanger. For a space restricted system, the model

00268-2 heat exchanger would work better due to its smaller footprint. Using the model 00268-2 heat exchanger also allows for easy configuration for different heat loads by simply changing the number of heat exchangers present in the system. Though for higher heat load systems (10+ kW), it may be necessary to use a larger shell and tube heat exchanger according to system flow rate. Because of the versatility of both of these heat exchangers, they should both be considered for use with the integrated recirculating target system and selected based upon the heat load required, and the space available.

System Modeling and Performance Simulation

The simulation for the prototype system was performed using ΔP vs. flow data on a 10 mm target body. The 10 mm target adds minimal pressure drop to the system amounting to around 1 psi at 2.20 LPM. Pressure drop data for the connection tubing can be calculated directly. The pressurizer acts to control system pressure and as a surge volume. The pressurizer does not contribute to the pressure drop in the system and therefore is not considered in the pressure drop calculations.

Single Shell and Tube Heat Exchanger System

The normal operating speed of the regenerative turbine pump during product production is anticipated to be between 4000 and 6000 RPM. Therefore, the performance of the system was considered only at that level. Two simulations were made for systems using a single shell and tube heat exchanger with 1/16" and 1/8" tubes. Figures 14 and 15 show the thermal performance data for these simulations. Table 2 displays the breakdown of volume for the systems as well as performance data at a pump speed of 5500 RPM and an MATD level of 125 °F.

From Table 2 it can be seen that the systems are within 3 mL of each other. Using a 15 mm target instead of a 10 mm target would increase the system volume by 0.90 mL. Performance varies greatly between the two simulated systems though the only difference is the connecting tube diameter. With nearly twice the heat transfer rate, over 3 times the flow rate, and only a 25% increase in volume the system with 1/8" connection tube diameter is more efficient. The increase in heat transfer rate is directly related to the lower pressure drop and higher flow rate associated with the larger tubes.

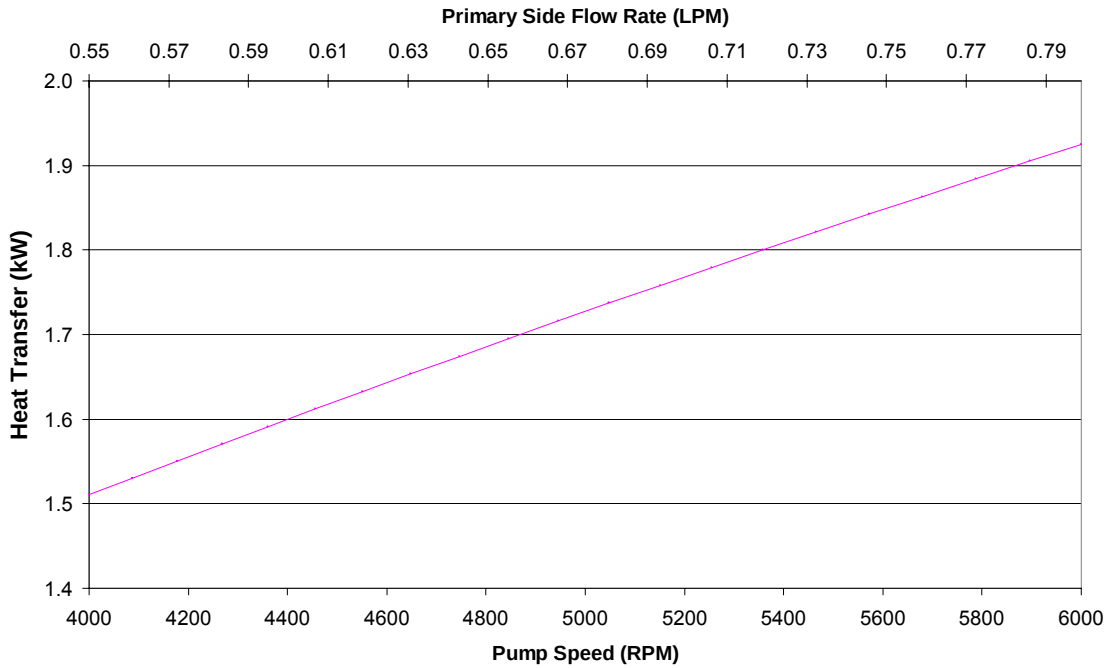

Figure 14: Simulation data for system with single heat exchanger system and 1/16" ID tubes, MATD = 125 °F

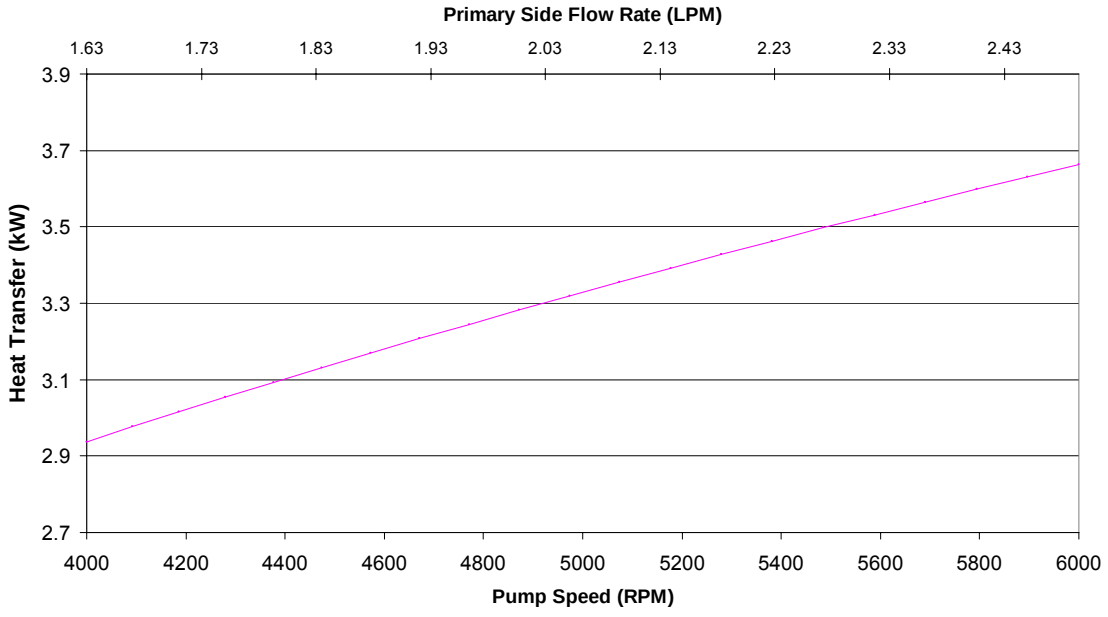

Figure 15: Simulation data for system with single heat exchanger system and 1/8" ID tubes, MATD = 125 °F

Table 2: Integrated system volume breakdown

Length of connection tubing (in) =	20	
Tube Diameter (in) =	1/16	1/8
System Volume Breakdown (mL):		
Connection tubing =	1.01	4.02
Primary side of heat exchanger =	2.01	
Heat exchanger manifolds =	0.40	
Target (10mm) =	0.70	
Pressurizer =	2.50	
Pump =	2.50	
Misc: Fittings, etc. =	3.00	
TOTAL VOLUME =	12.52	15.53
Primary side flow rate (LPM) =	0.73	2.27
Heat transfer rate (kW) =	1.82	3.50

Multiple Shell and Tube Heat Exchanger System

In cases where higher heat transfer rates are required, it may be necessary to use a set of heat exchangers in series. This will increase thermal performance of the system while only increasing volume by around 2.81 mL with 1/8" diameter tubes. Table 3 shows basic information for this system at a pump speed of 5500 RPM and an MATD level of 125 °F. Figure 16 shows the thermal performance data for this system between 4000 and 6000 RPM.

Table 3: Basic system information for two Exergy model 00268-2 shell and tube heat exchangers in series

TOTAL VOLUME (mL) =	18.34
Primary side flow rate (LPM) =	2.16
Heat transfer rate (kW) =	5.66

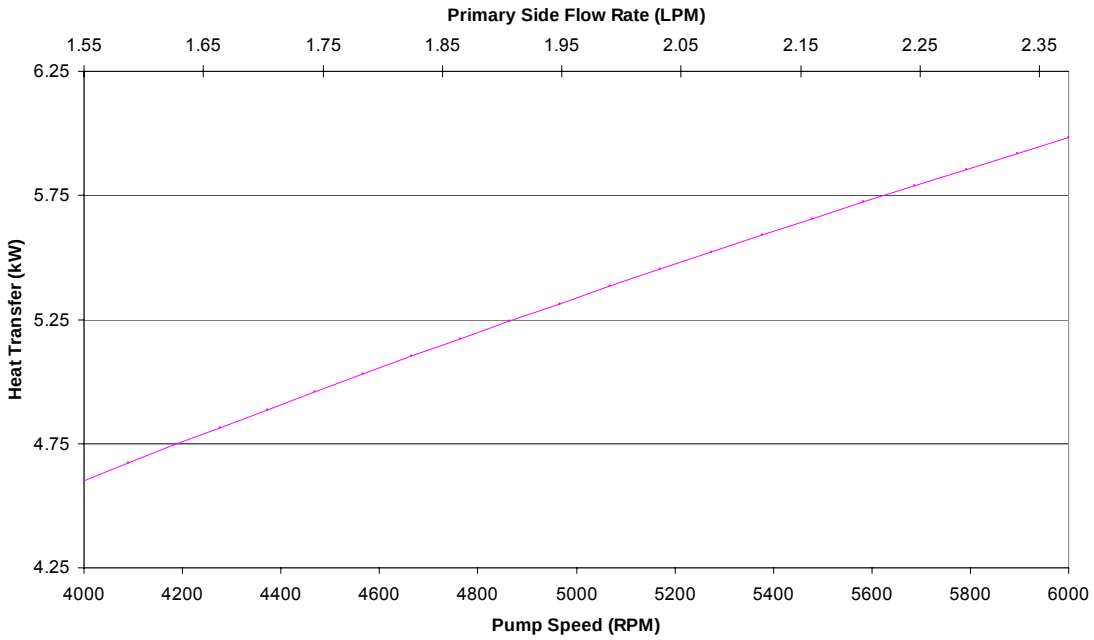

Figure16: Simulation data for system with two Exergy model 00268-2 shell and tube heat exchangers in series and 1/8" ID tubes, MATD = 125 °F

If even higher heat transfer rates are needed, it is possible to use a different model Exergy shell and tube heat exchanger. The Exergy model 00268-1 is the next size larger shell and tube heat exchanger built in the 10 series. Using two of these heat exchangers in series has a predicted heat transfer rate of 10.35 kW at a primary side flow rate of 2.37 LPM. Table 4 displays the basic information for this system at a pump speed of 5500 RPM and an MATD level of 125 °F. Figure 17 shows the thermal performance data for this system between 4000 and 6000 RPM.

Table 4: Basic system information for two Exergy model 00268-1 shell and tube heat exchangers in series

TOTAL VOLUME (mL) =	22.35
Primary side flow rate (LPM) =	2.16
Heat transfer rate (kW) =	9.75

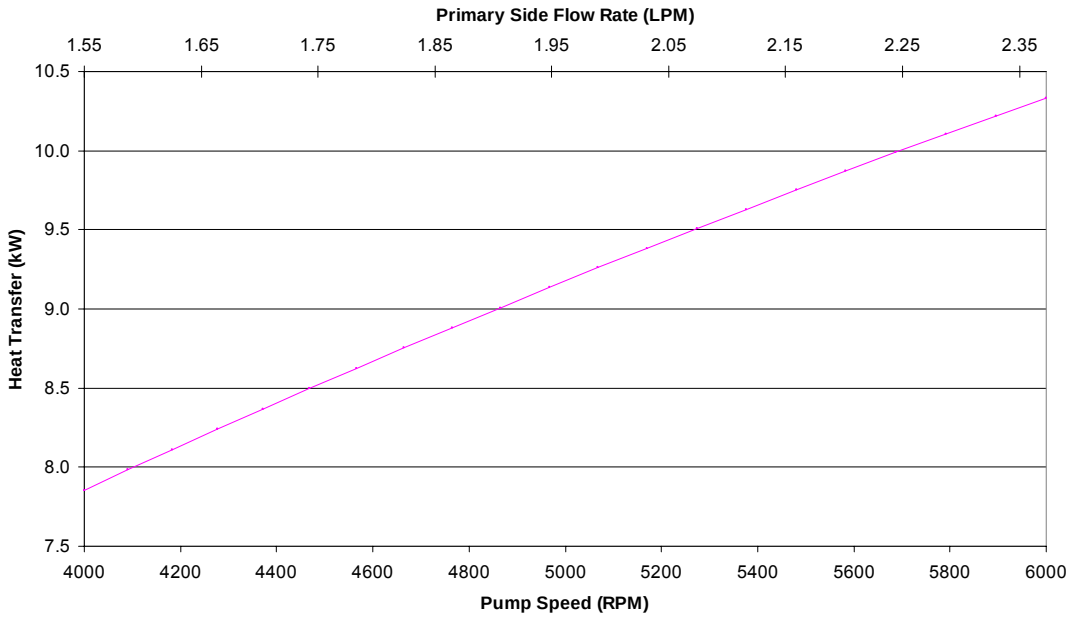

Figure 17: Simulation data for system with two Exergy model 00268-1 shell and tube heat exchangers in series and 1/8" ID tubes, MATD = 125 °F

Performance Prediction for a Commercially Available System

One possible difference in a commercial system is the elimination of some primary side connective tubing. Small ID tubes contribute a large portion of the total primary side pressure drop. The fittings used to connect components also add to the primary side pressure drop. A commercial system would likely include shortened tubes and welded connection points, thus decreasing the primary side pressure drop and increasing flow rate and heat transfer.

An estimated 4 inches of tubing is assumed necessary to connect the pump, heat exchangers, and target. This simulation considers the use of two Exergy 00268-2 shell and tube heat exchangers in series, with 4 inches of 1/8" ID connective tubing. Table 5 displays the basic information for this system at a pump speed of 5500 RPM and an MATD level of 125 °F. Figure 18 shows the thermal performance of this system for pump speeds between 4000 and 6000 RPM.

Table 5: Basic system information for a commercially available system using two Exergy model 00268-2 shell and tube heat exchangers in series

TOTAL VOLUME (mL) =	15.12
Primary side flow rate (LPM) =	2.66
Heat transfer rate (kW) =	6.38

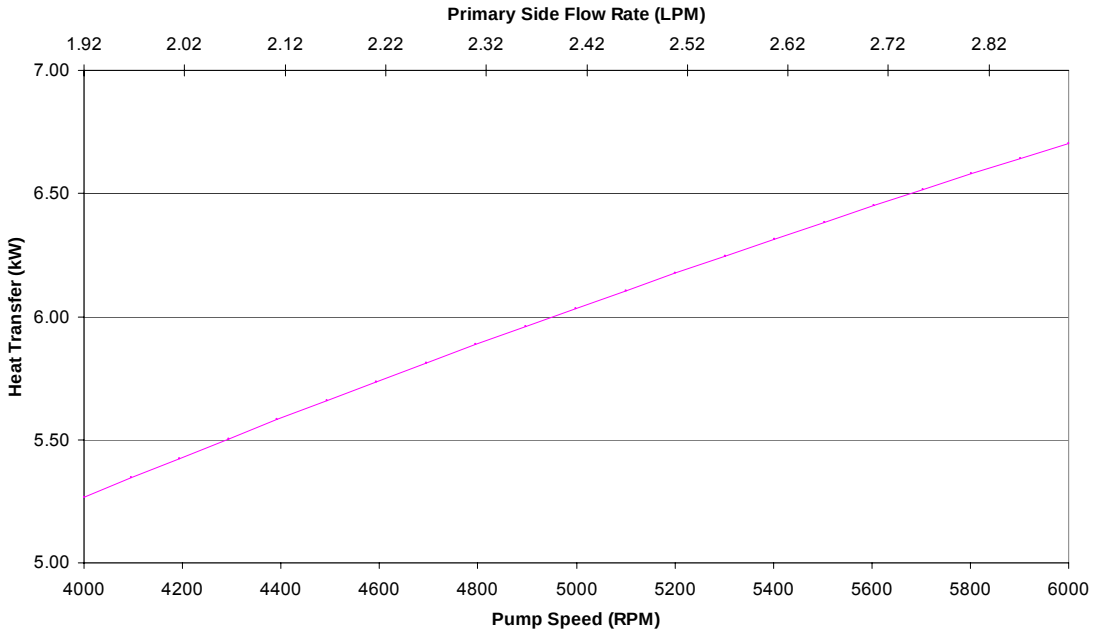

Figure 18: Simulation data for commercially available system using two Exergy model 00268-2 shell and tube heat exchangers in series and 1/8" ID, 4" long connective tubes, MATD = 125 °F

In comparison to a system with 20 inches of 1/8" ID connective tubing and Swagelok fittings, this system removes approximately 13% more heat with a 23% higher primary side flow rate.

Conclusions

This study examines two new heat exchangers for the integrated recirculating target system capable of providing sufficient heat removal capacity for high powered targets up to 10 kW. The experimental tests for both the shell and tube heat exchanger and the cross flow heat exchanger show that the computational models developed to simulate system performance are accurate and can be considered valid for future system simulations and heat exchanger designs.

Optimization studies identified the design characteristics desired in a prototype shell and tube heat exchanger. It was found that the commercially available Exergy 10 series shell and tube heat exchangers were equivalent in size scale to the optimized designs. The Exergy heat exchangers also incorporate materials that are compatible with the integrated recirculating target system. Even with the limitation of the maximum average temperature difference (MATD), which reduces maximum possible heat transfer rates, the Exergy heat exchangers still satisfy the design goals for a low system temperature and pressure. The Exergy model 00268-2 shell and tube heat exchanger was tested up to 5.9 kW with a primary side flow rate and volume of 6.7 LPM and 2.81 mL (with manifolds). It has a peak performance of 6.0 kW at a primary side flow rate of 7.5

LPM. Using a set of these heat exchangers in series allows for a maximum heat transfer rate of 10.5 kW with a primary side flow rate of 6.5 LPM.

Highly efficient designs such as the micro cross flow heat exchanger represent the best case scenario for a cross flow heat exchanger. For this study it was impractical to construct this type of heat exchanger due to complications with the construction techniques necessary to fabricate it. Future research and design of the integrated recirculating target system could include the development of a micro cross flow heat exchanger that may represent the most efficient design for a commercially available system.

The constructed prototype cross flow heat exchanger represents a trade off between maximum heat transfer and practicality. It was experimentally tested up to 7.2 kW at a primary side flow rate of 6.0 LPM. It has a peak performance prediction of 10.0 kW at a primary side flow rate of 7.5 LPM. The cross flow design relies on a high inlet temperature and system pressure in order to achieve maximum heat transfer. This means that the integrated recirculating target system would have to run hotter as a whole and higher pressures would be required to prevent boiling. In the future, it might be possible to construct a cross flow heat exchanger with smaller channel diameter and channel spacing as discussed with the alternate cross flow heat exchanger. This will increase the performance of the heat exchanger and allow for a reduced inlet temperature and system pressure. The alternate cross flow heat exchanger presented in this study with 0.030" channel diameter and 0.010" channel spacing has a peak predicted performance approaching 14 kW. If the cross flow heat exchanger design is pursued further, this is a viable design for construction and use.

The shell and tube heat exchanger was selected for use with the prototype integrated recirculating target system. Its selection was based on its performance and size. It out performs the current prototype cross flow heat exchanger at a moderate system pressure and temperature with less volume. Though the use of the Exergy model 00268-2 shell and tube heat exchanger requires two units to perform at higher heat loads, it is still more volume efficient that than the prototype cross flow heat exchanger.

At a maximum pump speed of 6000 RPM it is estimated that the integrated system can reject 3.65 kW of heat with one shell and tube heat exchanger at a primary side flow rate of 2.5 LPM and 6.0 kW with a set of shell and tube heat exchangers in series at a primary side flow rate of 2.37 LPM. For a higher capacity system using two larger Exergy shell and tube heat exchangers the integrated system could reject 10.35 kW of heat at a primary side flow rate of 2.37 LPM. These heat transfer rates are strongly dependent on primary side flow rate and could be sharply increased for both systems if pump performance is increased.

References

[1] Clark J.C. "High-Powered Cyclotron Recirculating Targets for Production of the ^{18}F Radionuclide." Masters Thesis. Department of Nuclear Engineering, North Carolina State University. December 2004.

[2] Ehrfeld W., Hessel V., Lowe H. Microreactors, New Technology for Modern Chemistry. Wiley-VCH, July 2000.

[3] Newnam, Robert P., "High Capacity Heat Exchangers for Recirculating 18F Radionuclide Production Targets," Masters Thesis, Department of Nuclear Engineering, North Carolina State University, 2007

[4] Exergy, LLC. Miniature Heat Exchangers. Garden City, NY. <http://www.exergyinc.com/> January 24, 2006.

[5] Holman J.P. Heat Transfer. McGraw-Hill Companies, Inc., Ninth Edition, 2002.

[6] Incropera F.P., Dewitt D.P. Heat and Mass Transfer. John Wiley & Sons, Inc., Fifth Edition, 2002.

[7] Kakac S., Liu H. Heat Exchangers, Selection, Rating, and Thermal Design. CRC Press, Inc., 1998.

[8] Schubert K., Bier W., Linder G., and Seidel D. Profiled Micro Diamonds for Producing Microstructures. Precision Machining, 1990.

[9] Wright B. Regenerative Turbine Pumps: Unsung heroes for volatile fluids. *Chemical Engineering*, 106(4):116, April 1999.